EMBRY-RIDDLE
Aeronautical University™
SCHOLARLY COMMONS

Doctoral Dissertations and Master's Theses

Spring 5-2016

Magneto-Rheological Fluid Device as Artificial Feel Force System on Aircraft Control Stick

Vignesh Manoharan
Embry-Riddle Aeronautical University

Follow this and additional works at: https://commons.erau.edu/edt

Part of the Navigation, Guidance, Control and Dynamics Commons

MAGNETO-RHEOLOGICAL FLUID DEVICE AS ARTIFICIAL FEEL FORCE

SYSTEM ON AIRCRAFT CONTROL STICK

A Thesis

Submitted to the Faculty

of

Embry-Riddle Aeronautical University

by

Vignesh Manoharan

In Partial Fulfillment of the

Requirements for the Degree

of

Master of Science in Aerospace Engineering

May 2016

Embry-Riddle Aeronautical University

Daytona Beach, Florida

MAGNETO-RHEOLOGICAL FLUID DEVICE AS ARTIFICIAL FEEL FORCE

SYSTEM ON AIRCRAFT CONTROL STICK

by

Vignesh Manoharan

This Thesis is prepared under the direction of the candidate's committee chairman, Dr. Daewon Kim and co-chairman Dr. Dongeun Seo, Department of Aerospace Engineering and has been approved by the members of the thesis committee Dr. David J. Sypeck, Department of Aerospace Engineering, Daytona Beach Campus and Dr. Yongho lee, Department of Mechanical Engineering, Daytona Beach Campus. It was submitted to the School of Graduate Studies and Research and was accepted in partial fulfillment of the requirements for the degree of Master of Science in Aerospace Engineering.
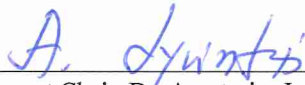
THESIS COMMITTEE

Chairman, Dr. Daewon Kim

Co-chairman, Dr. Dongeun Seo

Member, Dr. Yongho Lee

Member, Dr. David J. Sypeck

Department Chair, Dr. Anastasios Lyrintzis
or Graduate Program Coordinator, Dr. Eric Perrell

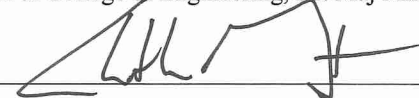Date 5/2/16

Dean of College of Engineering, Dr. Maj Mirmirani

Date 5/2/16

Vice Chancellor, Academic Support, Dr. Christopher Grant

Date 5/2/16

ACKNOWLEDGMENTS

TABLE OF CONTENTS

LIST OF TABLES

LIST OF FIGURES

SYMBOLS

τ	Shear stress
τ_y	Yield stress
H	Magnetic field strength
η	Coefficient of viscosity
$\dot{\gamma}$	Shear rate
F_d	Force obtained from the device
F_c	Force due to shear stress
$\dot{x}$	Velocity of the piston
C_0	Viscosity damping coefficient
V_t	Voltage
I_t	Current
R	Resistance
L	Inductance
k_H	Absorber gain coefficient
T_e	Electrical time constant
b_H	Gain coefficient
T_m	Settling time for MR fluid
B	Magnetic field intensity

ABBREVIATIONS

MR fluid	Magneto-Rheological fluid
FBW	Fly-by-wire
PU	Polyurethane
CAD	Computer Aided Design
PID	Proportion Integral Derivative
NI	National Instrument
DAQ	Data Acquisition
MRE	Magneto-Rheological Elastomer
SISO	Single Input Single Output
MISO	Multi Input Single Output
UTM	Universal Testing Machine

ABSTRACT

The conventional feel system in any aircraft occupies large space in the cockpit and has complicated designs. The primary objective of this research is to develop an artificial feel force system that can overcome some drawbacks of the current feel force system. A novel feel system using magneto-rheological (MR) fluid is constructed to precisely control the shear stress under the magnetic field. To validate the functionality of the MR artificial feel system, the final system is fabricated and multiple tests are performed to acquire force-velocity characteristics that are compared to the mathematical model derived. In addition, the reference model of the force feedback control is simulated for the feel force application. Both experimental and simulation results are compared to validate the derived system model. The system response time and the sampling rates are evaluated and compared to the conventional system at the end. It is concluded from the research that the developed artificial feel system can precisely control and acts as a fail proof system when incorporated with a modern fly-by-wire aircraft system.

1. Introduction

The research is in the field of artificial feel systems that are used in aircraft fly-by-wire technology. The prototype model in this research is designed to provide resistive force to the aircraft control stick by using Magneto-Rheological (MR) fluid device. This thesis will also discuss about the recent trends in the application of MR fluid. The properties of MR fluid are portrayed and the behavior of fluid to the magnetic field is studied from the prior arts. The evolution of artificial feel force system on aircraft is studied in detail and conventional techniques in providing artificial feel force on control stick are explained from the literatures.

1.1. Artificial Feel Force System

During the initial decades of controlled flight, the pilot's control stick was directly connected to the control surfaces on the aircraft. Therefore, the pilot was able to feel the aerodynamic forces acting on the aircraft surfaces when maneuvering the aircraft. This control force was provided by the pilot directly on control stick and this system also gave feedback to the pilot directly as an alert of a possible dangerous attitude of the aircraft. However, the fly-by-wire (FBW) control systems began to be implemented during the 1970s and they used boosters to actuate the control surfaces of big aircrafts. As a further improvement in convenience to the pilot in controlling the aircraft, artificial feel systems were designed. They are incorporated with the control systems to provide artificial force feedback, by using artificial feel devices. The schematic of current artificial feel force system used in the Airbus is shown in Figure 1.1(Artificial feel system, 2016).
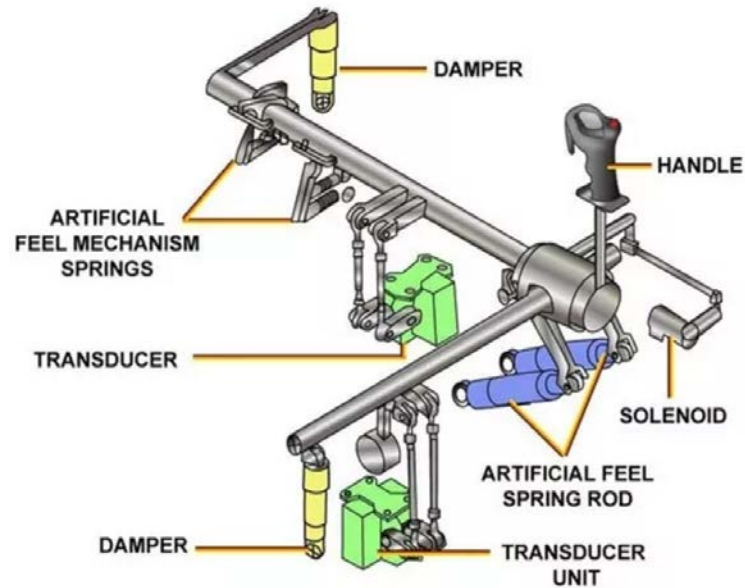
Figure 1.1 Conventional spring type feel system used in Airbus 320/340/360(Artificial feel system, 2016).

1.1.1. Prior Arts

An artificial feel force system for a control stick is presented by Griffith (1978). This system includes a non-linear or irreversible linkage apparatus coupled between the stick and a variable force gradient spring. This is the earliest stage of development in the artificial feel force devices. The system is bulky with complicated linkages, which ultimately required further improvements.

Another system is patented by Berthet and Bondivenne (1998) wherein the control stick is moved by an actuator controlled by the onboard flight computer. The position of the stick is varied using actuators in accordance with force and position data measured by sensors following a position vs. force law programmed into the computer. The major drawback of using this system is the possibility of the hydraulic system creating back pressure that could move the control stick automatically even if force is not applied to the stick.

An active control stick assembly is provided by Hanlon, Potter, and Wingett (2011). In this system, the active control stick assembly includes a housing assembly and a control stick support body mounted within the housing assembly which allows for rotation about two orthogonal and co-planar axes. A control stick is coupled to the support body and it rotates from a null position to a plurality of control positions. A spring element is also coupled between the housing assembly and the control stick support body, it passively biases the control stick toward the null position. The complete mechanism of servo motor operated artificial feel system with different components is shown in Figure 1.2.
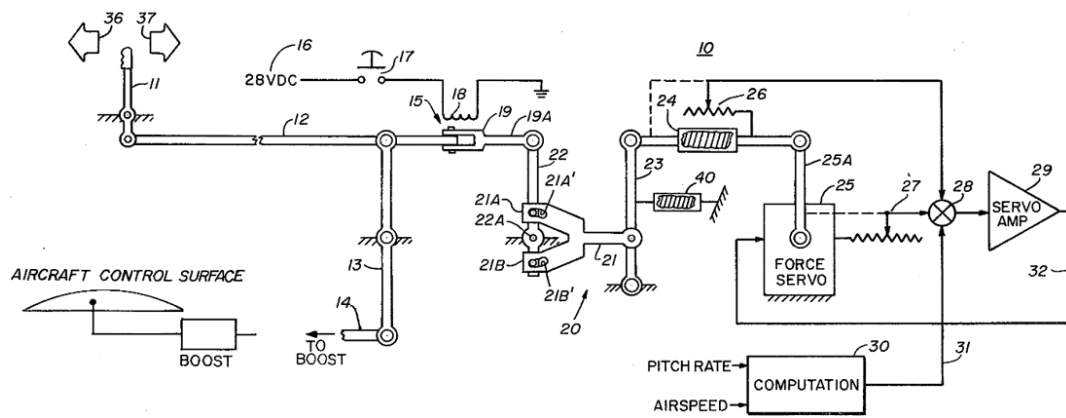
Figure 1.2 Schematic of the artificial feel system operating using servo mechanism
(Hanlon, Potter, and Wingett, 2011)

While recent patents are filed for different artificial feel force systems, none of them includes the use of MR fluid device as the artificial feel device. However, many scholarly journals have been published on modeling MR fluid properties and also in designing MR fluid devices. The most relevant of these papers are reviewed below.

One recent publication by Ahmadkhanlou, Mahboob, Bechtel and Washington (2012) derives an improved model to accurately simulate the MR fluid properties in actuators and sensors. This model is based on the kinetic energy theory and it assumes the

two MR fluid particles as a dumbbell system attached by a spring. It is concluded that this model greatly improves on the prediction of MR fluid shear stress before the yield point over previous models.

Another publication originally presented by Gavin, Hoagg and Dobossy (2001) at a workshop on using smart structures for seismic control presents fundamental equations and optimal design measures of merits when building an MR damper. This paper gives finite element analysis simulation results for an optimal design and also compares results obtained through experimentation to the simulated performance of the design. However, no publication is found about MR damper as an artificial feel device in aircraft control systems, which provides motivation for research in this specific field.

1.2.   Magneto-Rheological fluid

The MR fluid is a non-Newtonian fluid and contains magnetic particles suspended in a carrier fluid which is mostly vegetable oil. The fluid has very high viscosity especially when it is exposed to magnetic field and it behaves like a viscoelastic solid. The shear stress of MR fluid can be varied very precisely by changing the magnetic field intensity. The MR fluid has the ability to resist or to transmit force and can be controlled using an electromagnet which provides solution for several control based applications. The MR fluid is not affected by temperature and requires much less current for actuation depending upon the output force required. The MR fluid material behavior under magnetic field is shown in Figure 1.3.
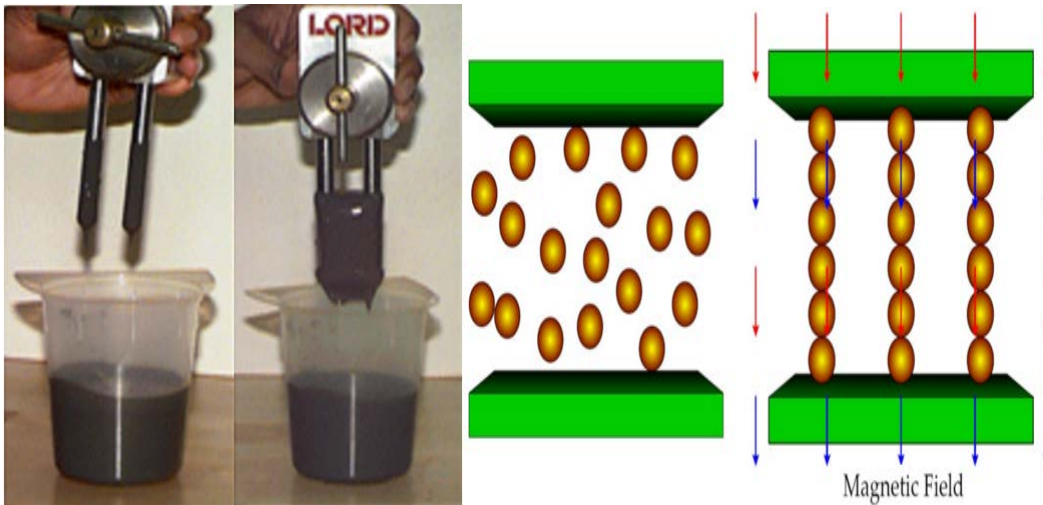
Figure 1.3 (a) MR fluid behaviour with and without magnetic field (Smart Materials, 2016) and (b) MR Particles alignment under magnetic field (Truong and Ahn, 2012).

1.2.1 MR fluid principles of operation

MR fluids can be operated in three modes such as flow mode, shear mode, valve mode. For many commercial applications, flow mode is preferred. In flow mode, both the walls are fixed and the fluid is made to flow through pressure. Application of magnetic field slows down the flow process. In shear mode, one wall is fixed and other wall moves with respect to the fluid in between two surface as shown in Figure 1.4 (a). This movement of upper surface creates shear force in the fluid and makes it flow. In the valve mode of operation, the pressure or force is applied in the top of the surface and the fluid is squeezed in between two surface. Three different modes of operation are shown in Figure 1.4 by Butz and Von Stryk (2002).
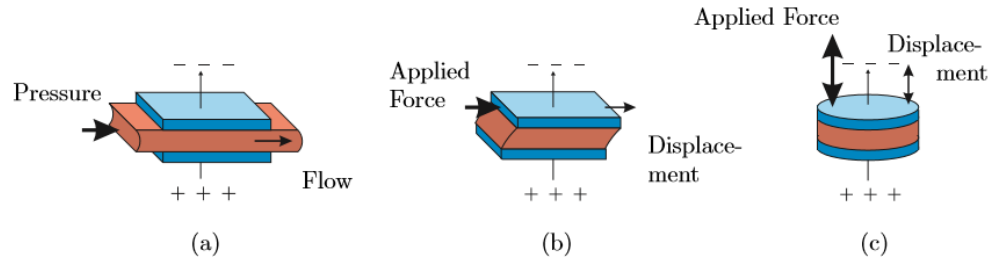
Figure 1.4 Three operational modes of MR fluid (a) flow mode (b) shear mode (c) squeeze mode (Butz and Von Stryk, 2002)

1.2.2 Magneto-Rheological devices

The Magneto-Rheological fluid device is gaining its importance in vibration suppression applications, control valves, haptic devices in medical field, and so on. The ability to control the device precisely with less power requirement and high durability with better operating temperature range are some of the significant advantages of this device for various engineering applications. A commercial design of MR device and the most common application of MR device is discussed further.

A force feedback device for robotic surgery from remote location is conceptualized and experimented by Neelakantan, Gregory and Randall (2002). The device provides haptic feel on the doctor's hands performing operation on the patient. On the other side the robot performs the operation on the patient. A special type of MR device using sponge is used for the low force requirement in this application. The device is modeled, fabricated, experimented and closed loop of the entire system is developed in this research.

Figure1.5 The picture of robotic surgery performed using MR dampers as force
feedback device (Wang, Yingru, 2006).

Recently, MR damper is used in vibration control of vibration control on bridge
cables by Sapiński, Snamina, Maślanka & Rosół (2006). This paper analyzes the vibration
characteristics of civil structures focusing on bridges. The damping of vibrations in the
cable stayed bridge is the primary objective in this research. The MR damper is fabricated
and the experimental setup is created. The vibration of the structure before using the
damper is measured first. Later, the vibration hotspots are monitored in the structures and
then the damper is deployed at these hotspots. The functionality of the damper is tested and
experimentally proved for the feasibility of concept. The picture of MR damper being used
in suspension bridge cables is shown in Figure 1.6.
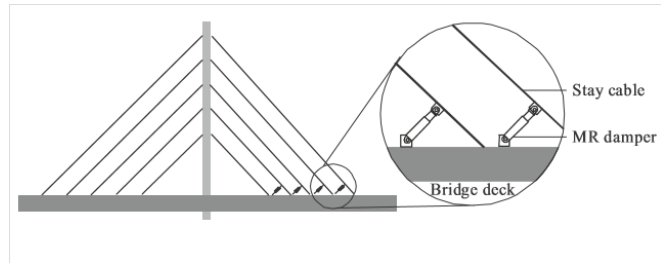
Figure 1.6 MR damper being used in cables of suspension bridges [12]

The MR fluids can also be incorporated in rotary devices which facilitates several applications in automobile industry. Recently Bucchi, Forte, Frendo & Squarcini (2013) proposed a novel idea of using MR fluid for automobile clutch application. The primary objective in this research is to minimize the energy absorption by vacuum pump for clutch operation. In this paper, a vacuum operated clutch is selected and compared with the hybrid vacuum MR fluid operated clutch. During braking, the driver pushes the brake pedal and the braking force on the tires are increased. This increase is based on the difference in oil pressure between two chambers which are the intake manifold in diesel engine and the atmospheric pressure. The operation of conventional clutch mechanism is briefly explained.

The significance of vacuum pump in disengaging the clutch is discussed and the replacement of friction operated clutch by MR fluid operated clutch is proposed in this research. To validate the concept, three prototypes of MR clutches are created incorporating permanent magnets for magnetization. The transmitted torque characteristics for engaged and disengaged mode of MR clutch is experimented for three prototypes and the energy absorbed from the vacuum chamber is monitored. The results from this research conclude that the MR clutch with hybrid vacuum pump can operate efficiently in extra urban environment with less braking operations. The clutch operated by MR fluid is shown in Figure 1.7 below.
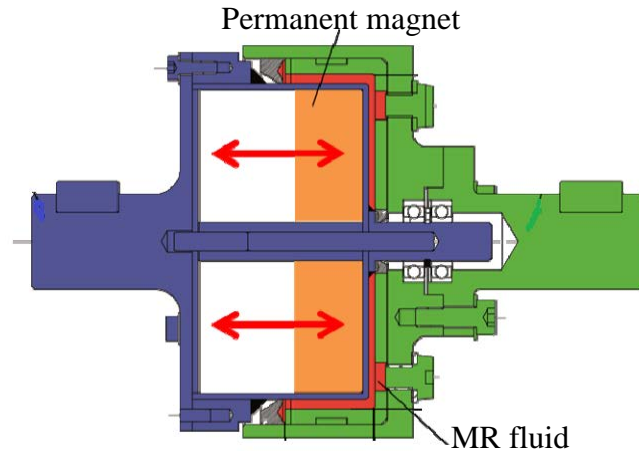
Figure 1.7 MR fluid operated clutch with permanent magnet (Bucchi, Forte, Frendo & Squarcini, 2013)

Avraam and Preumont (2009) worked on developing a muscular rehabilitant device using MR fluid. The device is constructed as a rotary MR actuator and the idea is found to be a novel innovation in its own field. The conventional muscle rehabilitant devices are huge and not compact enough to access all the body locations. This provides motivation for this research. The research provides solution for muscular evaluation of joints in the human body arms and signifies that it can be extended further to other joints. The paper lists out the application of MR fluids in prosthetic knees, muscle rehabilitants and other biomedical devices.

The paper briefly explains about the magnetic circuit design for the MR fluid actuator and analyze the magnetization effect from the device. The five different MR brake designs are studied and the significant advantages offered by each designs are included. The finite element modeling of different configurations of the device for specific magnetic flux is carried out and it is compared with the other designs. The real time data acquisition for the MR actuator is performed using torque sensor and strain gauges. The control operation of the MR actuator is performed using dSPACE controls. Several tests are

conducted to validate the compatibility of the prototype for medical application. Finally, a comparison between conventional rehabilitant device and MR fluid rehabilitant device is made. It is concluded from the paper that, the device developed using MR fluid offers more controllability, better performance and smaller in design for this specific application. The muscular MR rehabilitant device is shown in Figure 1.8.
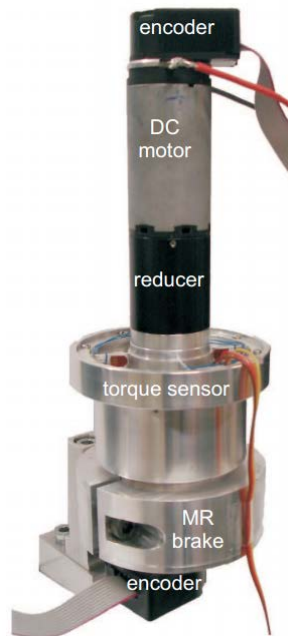
Figure 1.8 MR fluid muscle rehabilitant device (Avraam and Preumont, 2009)

Another rotary MR fluid brake is developed by Liu, Li, Kosasih, and Zhang (2006) for haptic force application. This research follows the same approach as that of constructing the MR fluid brake. Since the application is different, the design and mathematical modeling of the haptic device is found to be different from the conventional MR brakes. In this research the prototype design for the device is designed first and then analyzed using FEM software. The optimization in the design is made based on the flux distribution across the gap in the analysis results.

The real time data acquisition is performed using LabVIEW software and the device is precisely controlled using position feedback control. The potentiometer is used to find the position of the actuator at any time. The concept of using disk type MR fluid device for virtual reality application is validated in this research. The picture of haptic device with MR fluid actuator is shown in Figure 1.9.

Figure 1.9 MR fluid joystick for haptic force applications (Liu, Li, Kosasih, and Zhang, 2006)

Zhu (2005) worked on vibration isolation of rotary shafts using MR fluid dampers. The disk type MR dampers are used in this research, as the device is applied to rotary vibration control. Even though the MR disk type damper is operated in the same mode as that of previous applications, they can be used in multiple applications and also in various fields. Therefore, the paper explains that, this device operates on shear mode and Bingham model is used to model the device. Significantly in this research, the dynamic characteristics of the MR device are discussed in detail. The modes of vibration in the rotary shaft of the machine are observed and the device is built to suppress the vibration and also to vary the stiffness offered by the device.

The paper provides less information about the active vibration control in rotary shafts. It is concluded that the control operation for vibration reduction is investigated in the future. The paper also resolves that the nonlinear modeling of the disk shaped MR device is not carried out and remains as a future work in this specific field of research. The cross sectional diagram of MR rotor vibration control is shown in Figure 1.10 .
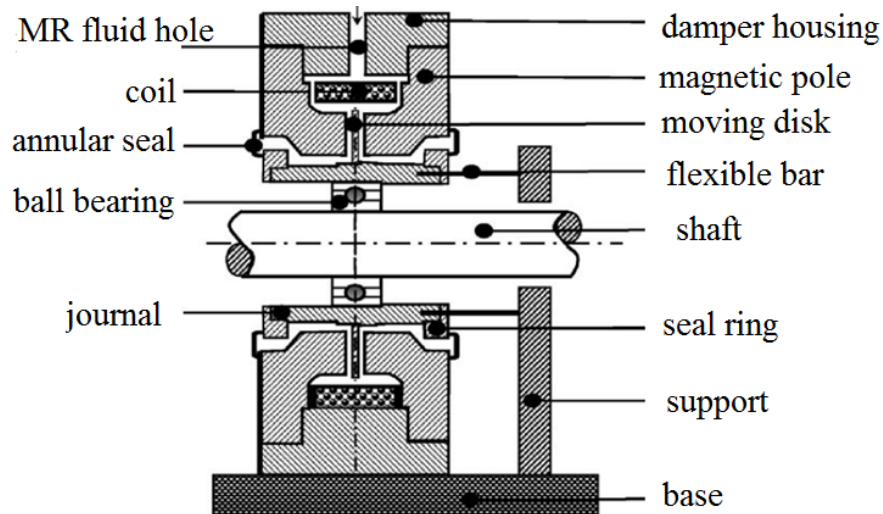
Figure 1.10 MR damper for vibration isolation in rotary shafts (Zhu, 2005)

The design of MR fluid damper for automobile suspension is done by Tu, Yang, He & Wang, L (2012). In this paper MR damper is called a smart damper and the semi-active vibration control is performed in vehicles. The single piston MR damper design is used in this research and the front end suspension of the vehicle is investigated. The basic equation for the magnetic field is derived and the design is analyzed in ANYS software. After the analysis, equation for the resistance force and the equation for energy storage are derived for the specific design. The MR damper is being tested in the UTM is shown in Figure 1.11.

Universal Testing Machine
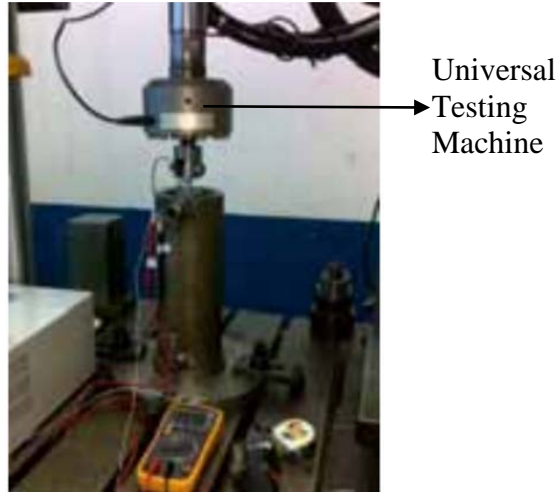
Figure 1.11 MR damper for automobile suspension mounted in the UTM (Tu, Yang, He & Wang, L.2012)

The design variables are identified from the mathematical equations and the fabrication of MR device is carried out in the next stage. The fabricated damper is tested for the predicted performance using a Universal Testing Machine. The damper is tested for different frequency modes and the force characteristics are recorded. The paper concludes that, the damper can operate in a semi-active mode for vibration control for automobile suspensions.

Carlson and Jolly (2000) published a paper on MR fluids that discussed the concept of MR elastomers and foam devices. Each part of the idea is elaborated and its's potential applications are discussed in the paper. The preparation and composition of MR fluids is first discussed and then continued by its properties. The MR fluid is a composition of ferrous particle at a range of 30nm diameter. The carrier fluid can be selected based on the stability of the fluid and the operating temperature. Carlson J. David is a senior research fellow at Lord Corporation and also a scientist working on MR fluid.

The MR fluid elastomer is considered to be a solid with polymer foam and MR fluid contained in it. This type of variable viscosity elastomer has several applications and has advantages over the magnetically controllable fluid. The paper signifies that the magnetically controllable elastomer is more stable and has better operating range than MR fluid. Another type of interesting application is MR fluid contained in a polymeric foam.

The foam material is made of Polyurethane and it has open celled structure. The pore size of the material provides the advantage of holding large number of Fe particles within the foam with less leakage. The absorbent matrix with MR fluid can be operated in shear mode and do not require any seals as conventional MR fluid device. The MR foam type devices are useful in low force requirement types applications.

Syman and Constantinou (1999) worked in protecting civil structures from seismic vibrations using MR dampers. The paper discusses about the different modes of seismic vibration control such as active, passive and semi-active vibration control. The emphasis is made on the semi-active vibration control and the advantages in this specific methodology is studied in detail. The passive vibration control requires no external power and performs the control operation in the structure. Seismic isolation system with flexible structure between the building and the system is demonstrated as an example for passive control. Figure 1.12 shows different components used in a MR damper.
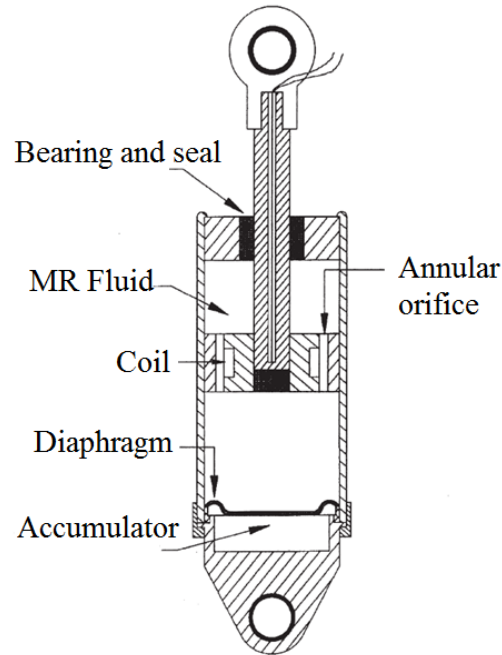
Figure 1.12 Components present in a MR fluid damper (Syman and Constantinou, 1999)

For an active control, large external power is required to generate the control forces. The control forces are generated based upon the feedback signal from the civil structure. The feedback signals are used to provide opposition force to the input forces and make the system stable. Usually a computer is used to record the feedback signal and it sends out the control signal to the external excitation.

The semi-active control offers the advantage of using very small external power in exciting the structure by getting feedback from the civil structures. The experimental testing of semi-active control is performed using a shaker table. It is concluded that the feasibility of achieving the semi-active vibration control using the MR fluid damper is validated and proved.

Grunwald & Olabi (2008) worked on developing a Magneto-Rheological valve for variable flow application. This research is useful in flow control applications and the paper discuss two different designs of MR fluid valves. The two different types of design are MRF valve and MRF orifice. In MRF valve the direction of flow is perpendicular to the external magnetic field. The principle of operation in MRF valve is shown in Figure 1.13.
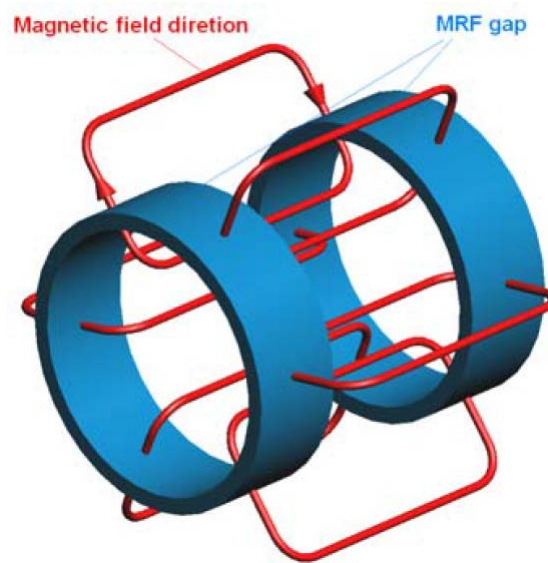
Figure 1.13 The magnetic field direction in MR fluid valve (Grunwald & Olabi, 2008)

In MRF orifice, the direction of flow is parallel to the magnetic field. The pressure drop across the valve and the orifice is theoretically derived and also experimentally verified. The experimental test rig is constructed for both configurations and it is concluded that the MRF valve offers more pressure than the MRF orifice, better and faster controllability with less leakage.
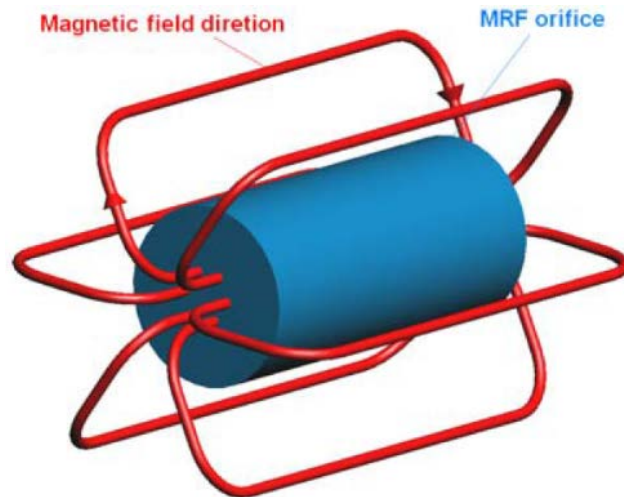
Figure 1.14 Magnetic field direction of MRF orifice (Grunwald & Olabi, 2008)

Deng, Gong & Wang (2006) developed a MR elastomer for adaptive tuned vibration absorption. This paper explains in detail about the manufacturing of MRE and also its composition. In this research the MRE along with the spring elements are mathematically modeled first. After deriving the numerical model with resonance frequencies, the prototype design is fabricated. The model is used in a beam with both ends fixed and the frequency attenuation is tested. The experimental results are compared with the numerical results and it is proved that the MRE can used in shock absorption than the passive shock absorber. The experimental setup with MRE is shown in Figure 1.15.

Figure 1.15 MRE experimental setup (Deng, Gong & Wang, 2006)

A novel idea of using MR damper for controlling the recoil dynamics of gun is studied by Mehdi and James (2001). The concept of using MR damper is experimentally tested and validated in this paper. Initially, the recoil dynamics is studied, the required stroke length and the velocity ranges are acquired. The advantage of using MR dampers in high velocity applications facilitates the idea for this recoil application. The MR damper is fabricated as a piston and cylinder and is attached to an experimental gun.

The MR fluid with two different flow principles are examined in this research and is shown in the Figure 1.16. The experimental setup is created such that the end of the recoil gun is attached to a piston of a MRF damper. The real time data acquisition is performed by using sensors such as LVDT and force transducer. The recoil demonstrator is selected such that the velocity of recoil is same as real time gun recoil velocity.
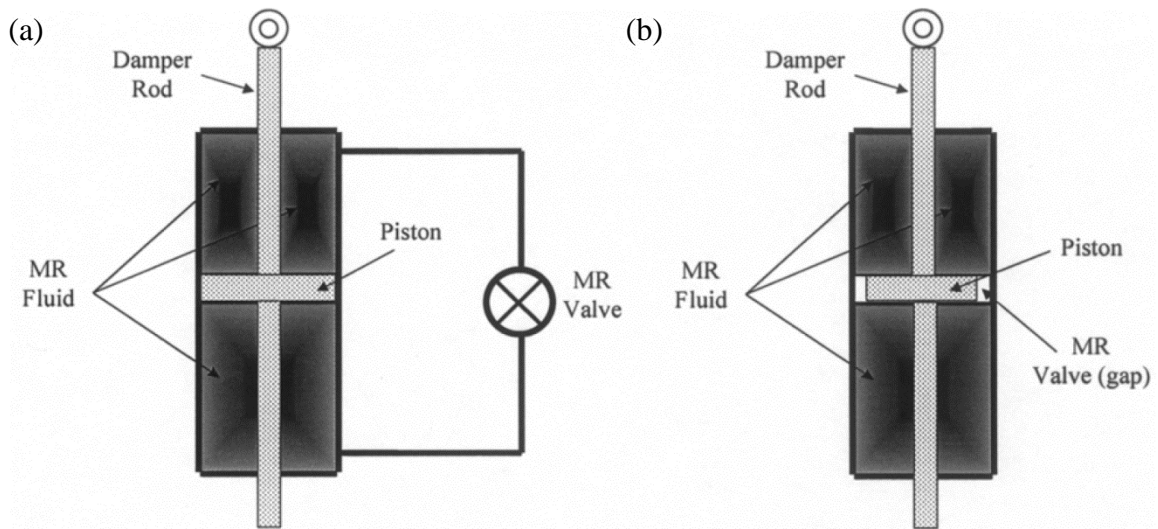
Figure 1.16 Two modes of MR fluid device operation (a) external (b) internal (Mehdi and James, 2001)

The MR device is tested for the damping characteristics in the field experimentation and the feasibility of using MR damper is experimentally proved. However other areas of research which includes modeling the damper and providing active control for recoil

applications are not discussed in this paper. The experimental setup for gun recoil damping

is shown in Figure 1.17.
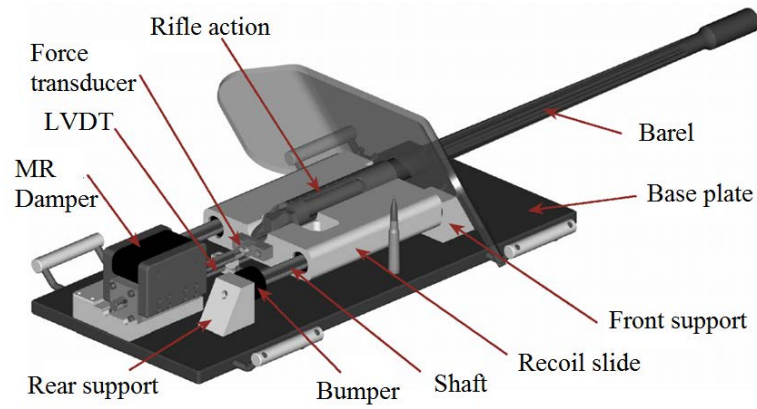
Figure 1.17 The experimental setup for gun recoil damping (Mehdi and James, 2001)

2. Objective and Approaches

The objective in this research is to design a simpler construction scheme for feel force system providing the artificial feel force to the pilot's control stick. The conventional feel system in aircraft include multiple components and mechanical linkages.

The improved reliability and response time of the developed system are also important parameters that are investigated during this research. If the device response lags behind the control stick movements, it can affect the pilot's ability to feel the haptic force. Also, investigating the response time of the system can allow for the determination of the maximum sampling rate that the computer can use in determining the position of the control stick.

The viability of applying this research in building the next generation of fly-by-wire systems can also be determined. Since the aircrafts built today are operated by digital systems, they have onboard computer systems. Hence, this MR feel system can be easily added to the flight control system. The research flow chart with the forecasted stages of research is shown in Figure 2.1.

The objectives in this research are carefully listed and the different phases of work and developments are forecasted in the initial stage. The concept is first experimented in the lab and the principle to operate the MR fluid for this application is experimentally verified. Later, the selection of specific MR device for the required force characteristics is examined. Design of experiment with two type of MR device design is performed.

Mathematical model

CAD Design

Fabrication

Experimental
validation

Simulation of
model

System development

System testing
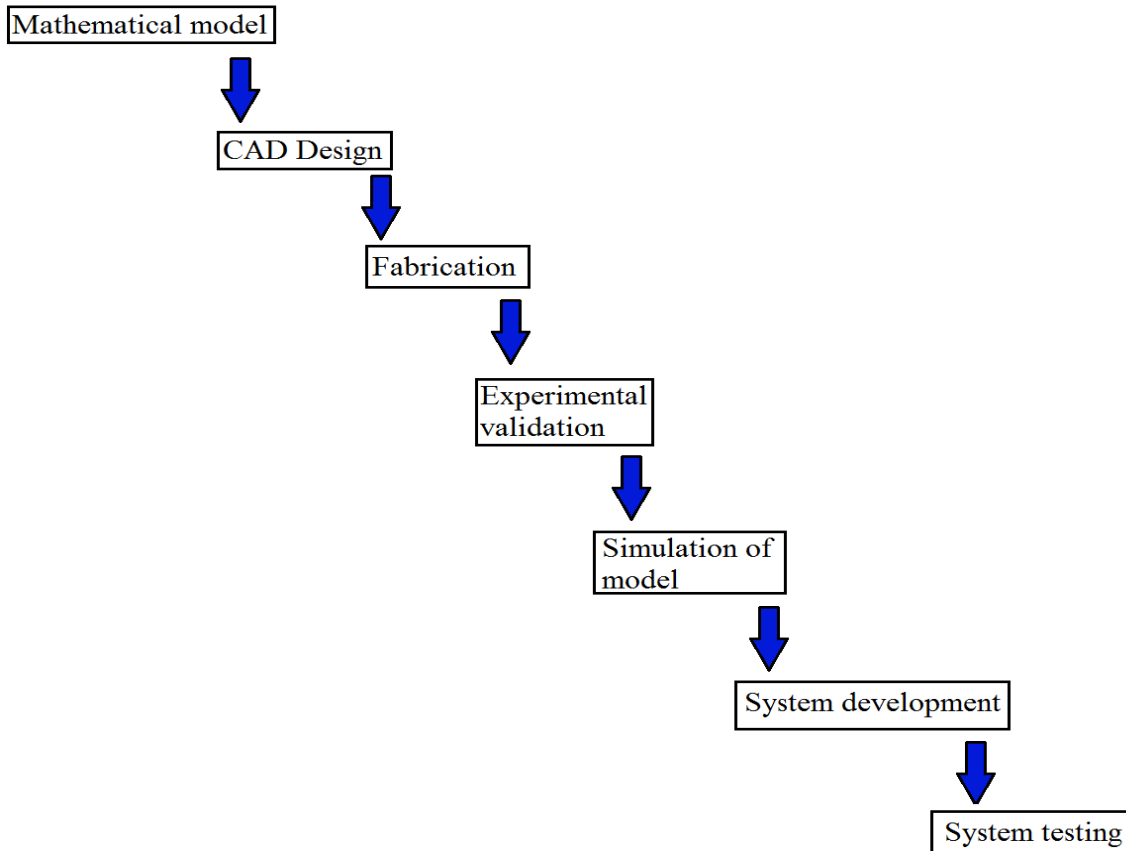
Figure 2.1 The research flow chart with forecasted stages in research

The preliminary design is selected and the CAD model is developed in CATIA V5. Once

the device is designed, the model is validated in ANSYS magneto static analysis. The 2D

Axi-symmetric model is analyzed to visualize magnetic flux distribution inside the device.

Based on the simulation results, the design can be further altered for specific

magnetic flux directions. The device is fabricated as piston and cylinder and the material

for storing MR fluid is chosen. The fabricated device is experimentally tested to verify the

force characteristics and functionality. The fabricated device is mathematically modeled

by making approximations and assumptions from the literatures.

3. Mathematical Modeling

The MR artificial feel device can be manipulated electronically by changing the magnetic field in the device. The MR fluid can be operated in different modes as explained in section I. However, the haptic device for feel force system is designed to be operated specifically in the shear mode and the control parameter is viscosity of the MR fluid. Therefore, the selection of an appropriate model for replicating the mechanical characteristics of the device is required.

Braz and Barros (2012) described the challenges in modeling the MR fluid device by listing out the uncertainties faced in the modeling approach. The paper also explained different modeling methodologies for MR devices. It is concluded in the paper that the Bingham plastic model is the basic model for MR fluid. It also mentions about the non-linear behavior and controlling characteristic in the Bingham numerical model. The dynamic and parametric modeling methodology is selected from Braz and Barros (2012) and followed in the MR artificial feel system research to simplify the modeling approach of MR device. The modeling approach followed by Braz and Barros (2012) provides sufficient validation for model selection and Bingham model is chosen for this specific feel system application with certain assumptions, which are made based on the mechanical characteristics of the device. Some of the commonly used modeling techniques are discussed below.

3.1. Kinetic theory model

Ahmadkhanlou, Mahboob, Bechtel & Washington (2009) work on using MR fluids in developing haptic tele robotic arm describes a novel modeling technique. The mathematical modeling technique is called Kinetic theory model. This model describes the

circular *Fe* particles in the MR fluid as dumbbell. There is a gap between two MR particle and they are elastically linked or plastically linked with each other. The mathematical equation governing flow, stress and particle orientation of the MR fluid is derived by integrating the above parameters of the equation over volume and carrier fluid. The paper considers the elastic dumbbell model and MR fluid iron particles are considered as dumbbell with mass m and connected by a spring. The rate of change of orientation of iron particles with respective to time can be given by Equation 1.

$$q_i = \left((L_{ij} - \mu D_{ij})q_j\right) + a_{ij}\frac{2kT\partial}{\Psi\partial q_k}\left(\xi_{kj}^{-1}\Psi\right) + 2a_{ij}f_j + a_{ij}(f_{1j}^{(m)} - f_{2j}^{(m)}) \qquad (1)$$

The orientation of the particle in Langrangian time derivative is given by q_i. The particles are considered to be elastic with modulus β and the stress tensor for the iron particles and carrier fluid is given by

$$\tau_{ij} = -p\delta_{ij} + 2\eta_s D_{ij} + n\beta\langle q_i q_j\rangle + \frac{c\dot{\gamma}n}{2(1+\chi)\sqrt{H_k H_k}}\langle q_i q_j\rangle - nkT\delta_{ij} \qquad (2)$$

where $$D_{ij} = \frac{1}{2}\left(L_{ij} + L_{ji}\right)$$

In these equations, τ_{ij} is the stress in the fluid, p is the constraint pressure that maintains incompressibility, δ_{ij} is the anisotropic Brownian motion tensor, η_s is the solvent viscosity, n is the particle number density, β is the dumbbell link spring constant, $\langle q_i q_j\rangle$ is the orientation of the particles averaged over a large region, c is the particle magnetization parameter, χ is the particle magnetic susceptibility, k is Boltzmann's Constant, T is the temperature and L_{ij} is the velocity gradient tensor. The kinetic theory model with two beads are shown in Figure 3.1.
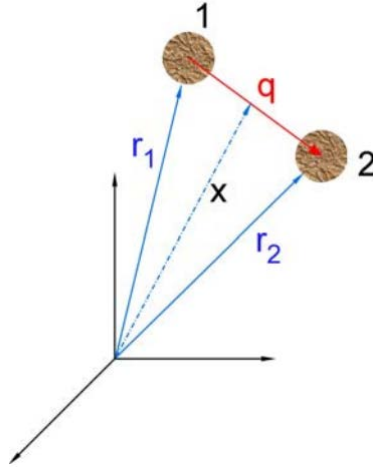
Figure 3.1 Kinetic theory model with MR particles as dumbbell 1 and 2 (Ahmadkhanlou, Mahboob, Bechtel & Washington, 2009)

It can be seen from the Figure 3.2 that the kinetic theory model follows experimental data much more closely than the other well-known and commonly used models. However, this accuracy comes with an increased complication in the formula used to find the shear stress. The kinetic theory based model requires many more values and knowledge of tensor mathematics to determine the shear stress. However, this equation can be greatly simplified if it assumed that the shear stress is in the presence of a transverse magnetic field, which is a good approximation for a simple MR damper design with a small gap of MR fluid outside a relatively large piston. The shear stress offered by the particle is given by Equation 3.

$$\tau_{12} = \eta_s \dot{\gamma} + \frac{nkT\zeta\dot{\gamma}}{4\left(\beta + \left(\frac{c\dot{\gamma}}{2(1+\chi)H}\right)\right)} \tag{3}$$

where ζ is the one dimensional analogy of a friction tensor and is a function of the magnitude of the applied magnetic field H, as defined in Equation 4.

$$\zeta(H) = 96402e^{(-4\cdot10^{-6})H} \tag{4}$$
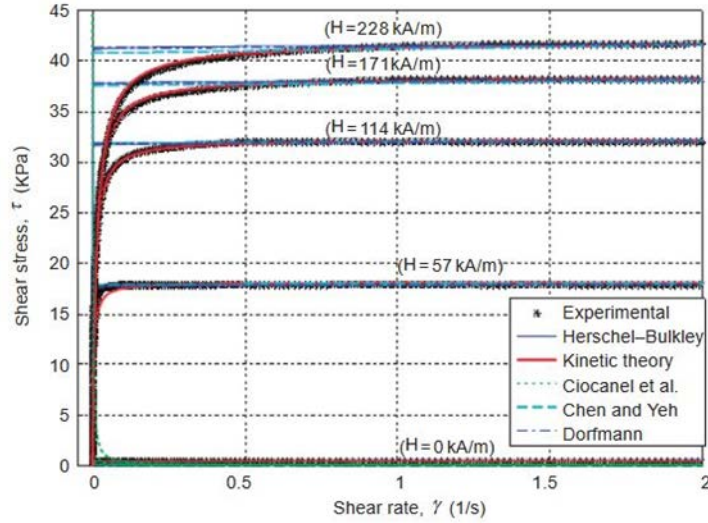
Figure 3.2 Kinetic theory data compared with the experimental shear stress data
(Ahmadkhanlou, Mahboob, Bechtel & Washington, 2009)

3.2. Bouc-Wen hysteresis model

Talatahari & Rahbari (2015) worked on modeling the hysteresis behavior of MR fluid device. In this paper traditional Bouc-Wen model is used and it is compared with an improved Bouc-Wen model. The Bouc-Wen model is used to demonstrate the nonlinear hysteresis behavior of the MR fluid. According to this model the nonlinear force offered by the device is given by Equation 5.

$$F = \alpha z + c_0 \dot{x} + k_0 (x - x_0) \tag{5}$$

where α is the Bouc-Wen model parameter, k_0 and c_0 are spring stiffness and dashpot damping coefficient, z is the hysteretic deformation which can be given by

$$\dot{z} = -\gamma |\dot{x}| z |z|^{n-1} - \beta \dot{x} |z|^n + A\dot{x} \tag{6}$$

Where A, β and γ are the Bouc-Wen model shape parameters. The mechanical Bouc-Wen model with hysteresis parameter is shown in Figure 3.3.
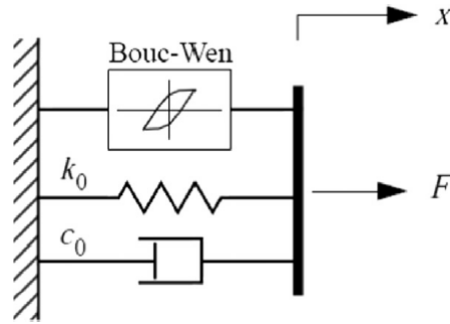
Figure 3.3 Mechanical model of Bouc-Wen hysteresis model (Talatahari & Rahbari, 2015)

The work done by Spencer, Dyke, Sain & Carlson (1997) explains the linearity of the hysteresis unloading and the smoothness of the transition from the pre-yield to post-yield region can be achieved by adjusting the parameters A, β and γ. The paper concludes that the Bouc-Wen model better describes the force-displacement behavior. It is also proved that the force-velocity response closely matches with the experimental data but it cannot provide sufficient data about the device operating in the low velocity ranges. The mechanical model of the improved Bouc-Wen model with extra parameters used to predict the damper behavior in the low velocity ranges are shown in Figure 3.4.
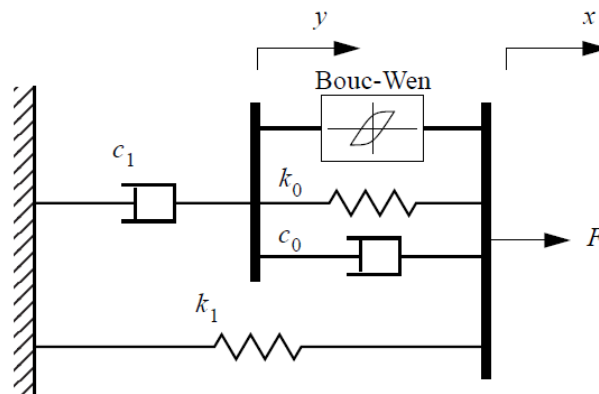
Figure 3.4 Improved Bouc-Wen model with hysteresis parameter (Spencer, Dyke, Sain & Carlson, 1997)

3.3. Herschel-Buckley model

The Bingham plastic model is modified to include MR fluid's classification as a shear thinning fluid in the Herschel-Buckley model. This modification is done through the use of the Herschel-Bulkley's viscoplastic model, which is first introduced in 1926 by Ahmadkhanlou, Mahboob, Bechtel & Washington (2009). This addition replaces the constant effective bulk viscosity of composite system term with a power law term which is dependent on the shear-strain rate, as shown in Equation 7.

$$\tau = \left[\tau_y(H) + K|\dot{\gamma}|^{\frac{1}{m}}\right] sgn(\dot{\gamma}) \tag{7}$$

where m and K are constants unique to the fluid. Unfortunately, this model is not ideal when designing an MR damper due to: (1) their macro scale basis, thereby treating the fluid as a single continuum, (2) the fact that the coefficients m, K and τ_y are found from the bulk properties of MR fluid and (3) the error that arises at low stress values. This third issue is of particular importance in the design of an MR fluid artificial feel force device for aircraft flight control systems. It will be shown later, the maximum force required to be provided to the control stick is relatively small when compared to the force generated in MR dampers that are being used in the automotive and construction industries. Therefore, even for small devices, the shear stresses required to be generated are very small. However, the above equations assume MR fluid as a solid below the yield point of the fluid. Therefore, this modeling approach is neglected.

3.4.   Bingham plastic model

The Bingham model by Bingham (1922) includes non-Newtonian characteristic of the fluid in the first part and the Newtonian behavior of the MR fluid in the second part of the equation. The shear stress offered by the MR fluid is given by Equation 8.

$$\tau = \tau_y(H) + \eta \dot{\gamma} \tag{8}$$

where τ_y is the yield stress offered by the fluid, H is the magnetic field intensity, η is the effective bulk viscosity of composite system, and $\dot{\gamma}$ is the shear rate of the fluid. The Bingham mechanical model of the device is shown in Figure 4. The basic shear stress equation is used to model the MR feel device with approximations. The mechanical Bingham model contains Coulomb friction was proposed by Maślanka, Marcin, Sapiński, and Snamina (2007) element along with the viscous element, as shown in Equation 9.

$$F_d = F_c \, sgn(\dot{x}) + C_0 \, \dot{x} \tag{9}$$

where F_d is the force offered by the damper, F_c is the Coulomb friction element, $\dot{x}$ is the piston velocity, and C_0 is the dynamic viscosity constant. The mechanical Bingham model with dashpot and spring system is shown in Figure 3.5.
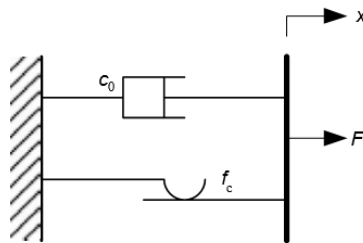

Figure 3.5 Mechanical Bingham model (Maślanka, Marcin, Sapiński, and Snamina, 2007)

Several assumptions are made in the Bingham modeling approach based on the mechanical characteristics of the feel force device, as listed here. First, the MR fluid

operating area is considered to be the gap between the sponge and the cylinder wall. The MR fluid operates in the shear mode within the gap and there is no porous flow of fluid between the cells in the polyurethane foam. Also, the velocity profile is linear for the MR fluid in the gap as the size of gap is negligible compared to the width of cylinder as shown in Figure 3.6. In addition, it is assumed that the foam undergoes nonlinear deformation inside the piston and the device provides no hysteresis.
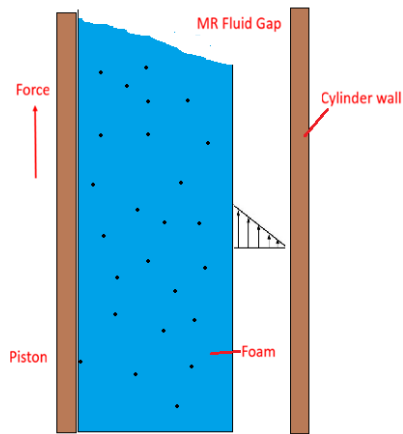
Figure 3.6 Schematic of cross section of the MR device with MR fluid gap

The Bingham modeling approach is followed with the aforementioned assumptions compromising the accuracy of the modeling behavior of the device. Later, the numerical model is simulated and the results are compared with the experimental results to validate the modeling approach in the later stage.

3.5.   Electrical equation and yield stress

The piston has coils wound up in a steel core and these coils act as an electromagnet. The electromagnetic circuit is considered as a solenoid with current and voltage as input parameters. Various magnetic field intensities can be obtained with different input current values and the number of wire turns. An electrical circuit model of the solenoid is derived

from the basic Ohm's law equation, neglecting the capacitance part and including only the inductance, resistance and current by the Equation 10 by Kenny (2011).

$$V_t = I_t R + L.di/dt \tag{10}$$

where L is the inductance in the circuit. The Laplace transform of the above equation is made to derive the state space equation of the electric circuit and the final equation with voltage in the coil is given by the Equation 11.

$$H(s) = [k_H/(T_e.S+1)]V(s) \tag{11}$$

where k_H is an absorber gain constant given by Milecki and Mikołaj (2012) with the resistance offered by the electric circuit, T_e is the electrical time constant ($T_e=L/R$) given by Gavin, Hoagg and Dobossy (2001), and $V(s)$ is the voltage from the coil.

Applying the Laplace transform to the yield stress variable to the first part of equation, we get the yield stress as a function of the magnetic field in state space equation, where τ_y is converted into first order transfer function model.

$$F_d = \tau_Y(H)$$

$$F_d = [b_H/(T_m+1)]H(s) \tag{12}$$

where b_H is the gain coefficient of force generated by the device, T_m is the time constant that is the time taken by MR fluid to react, and H(s) is the magnetic field.
The force offered by the device F_d is given by Milecki, Andrzej and Mikołaj (2012).

$$F_d = \left(\frac{b_H}{T_m S+1}H(s)\right)sgn[s.y(s)] + b_v[s.y(s)] \tag{13}$$

Substituting the above equation, we get,

$$F_d = \left(\frac{b_H k_H}{(T_m S + 1)(T_e S + 1)} V(s) \right) sgn\,[s.\,y(s)] + b_v[s.\,y(s)] \qquad (14)$$

The above equation is the final model for the MR fluid device that is to be used in artificial feel system and the value for the constants k_H, b_H, T_m and T_e are chosen based on the approximations made from the experiment and they are further used in the simulation.

4. MR Damper Design

The preliminary design for the MR damper is developed in CATIA V5. The literature review is conducted to identify the specific damper design suitable for the feel system application. The research work done by Poynor, James (2001) explains different types of MR damper designs. The paper also explains about twin tube and mono tube damper design with different construction.
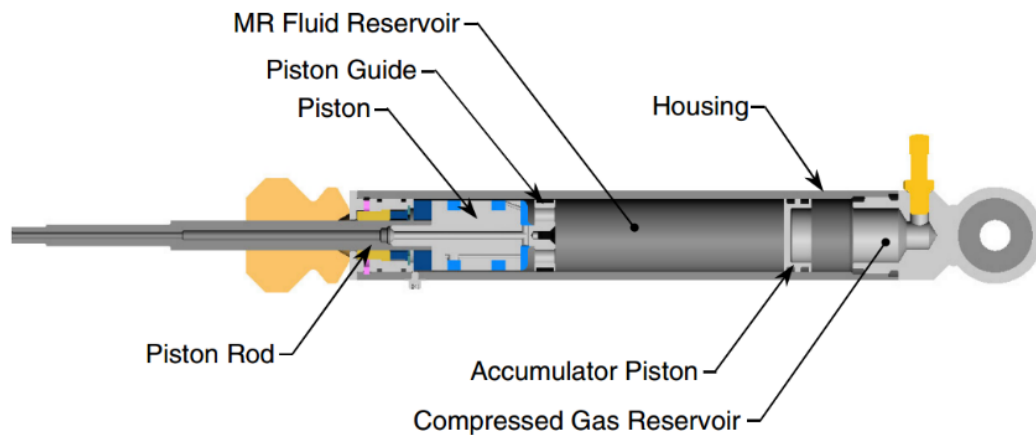
Figure 4.1 Cross section view of monotube MR damper with accumulator (Poynor, James, 2001)

Figure 4.1 shows the construction and the components present in a monotube MR damper. The paper also discusses on the potential applications of each damper design. It is concluded in the paper that the MR damper with monotube and twin tube configurations are suitable for applications like earthquake damping in buildings, automotive vibration damping, gun recoil damping. It can be understood from the literature that these applications require higher damping characteristics and more force, which results in complicated damper design. Therefore, these damper designs are validated to be unfit for feel force application.

The work done by Gavin, Hoagg & Dobossy (2001) determine the shear stress offered by a MR damper. This strategy is specifically developed for the MR damper designs that can be used for the control of building motion during seismic activity. The design variables are derived and individual parameters present in the equations are discussed in this paper. In this journal, a relationship is given between the total pressure drop across the piston and the shear stress acting on the piston. The pressure drop in the cylinder is given by the Equation 15 and 16.

$$\Delta p \approx 2.1 \frac{\tau_{ij}}{t_g} + \Delta p_N \tag{15}$$

$$\Delta p_N \approx \frac{12 Q \eta (2N_S) L_p}{\pi (D_p + t_g) t_g^3} \tag{16}$$

where t_g is the gap thickness, 2.1 is an empirically found correction factor for MR fluids, Q is the volumetric flow rate, N_S is the number of spools of wire forming the coil, L_p is the length of the piston poles and D_P is the diameter of the piston. To determine the shear stress needed, the equation may be solved for τ_{ij}. However, the total pressure drop now must be calculated. Fortunately, because it was determined that this design would be capable of generating a maximum force of 20 lbs, the above equation can be used to determine the required total pressure drop needed across the piston to generate this force.

$$F = \Delta p \pi \frac{\left[(D_P + t_g)^2 - D_r^2 \right]}{4} \tag{17}$$

where D_r is the piston rod diameter. To determine the volumetric flow rate, assuming the fluid is incompressible, the equation 18 gives the volumetric flow rate.

$$Q = V_p \left(\frac{\pi}{4} \right) (D_P^2 - D_r^2) \tag{18}$$

where V_P is the piston velocity. Using basic dynamics, the piston velocity is simply

$$V_p = \omega R \tag{19}$$

where ω is the angular speed of the joystick and R is the distance from the rotation point of the joystick in the base to the attachment point of the piston rod on the joystick.

Michael and David (2001) innovated a unique damper design with simple construction. The paper discusses about the application of MR fluid damper to washing machine vibration damping. The primary objective in this feel system research is to develop a damper design for low cost and lesser force damping characteristics. A novel way of storing the MR fluid in an absorbent matrix is performed by Michael and David (2001) and the idea is commercialized. The construction of this sponge type damper is found very simple and number of components in the device is less compared to the standard MR damper designs. Therefore, this design strategy is selected for the feel force application and the important construction and design procedures are followed from this literature.
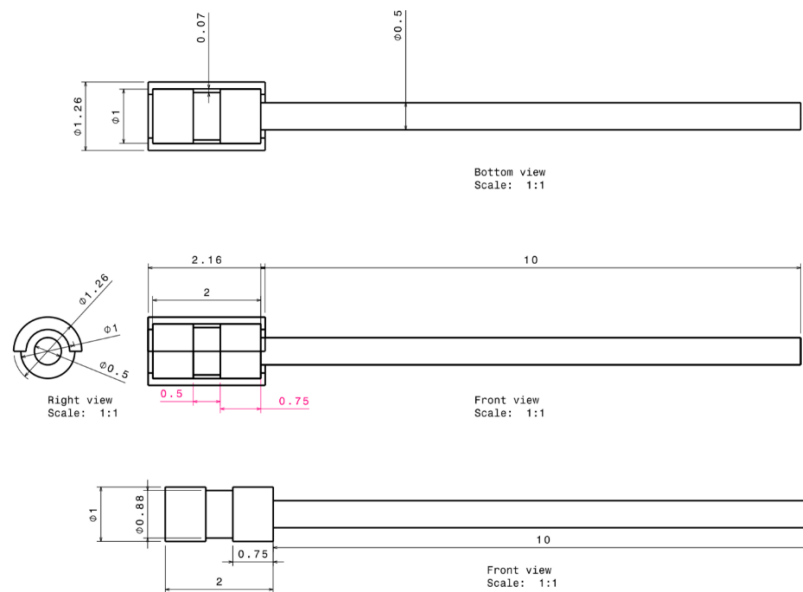

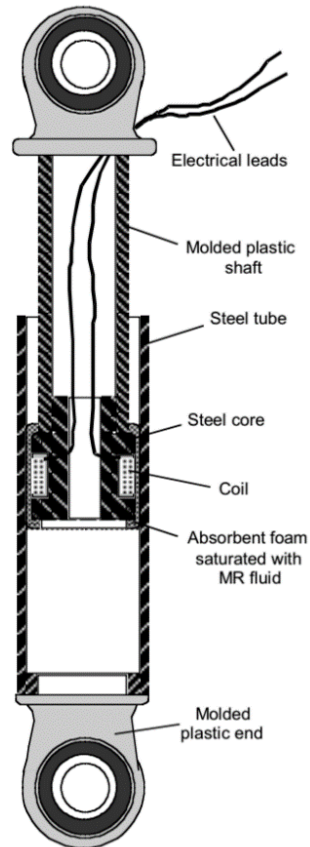Figure 4.2 Preliminary MR damper with sponge design with coil winding gap

Figure 4.3 Cross-sectional view of MR damper with sponge design [20]

The MR device is designed as a simple hollow cylinder with piston. The preliminary design of the MR damper piston with sponge is shown in Figure 4.2. Figure 4.3 shows the MR damper with the foam. The gap in the piston has coil windings and this functions as an electromagnet when the current is supplied. A special type of bond called (Cyberbond 2026) is used to bond the foam with steel core. However, since the gap provided in the piston is too small, the number of coil windings in the gap is not sufficient to generate required magnetic field. It is also understood from the ANSYS analysis and experimentation that the magnetic field direction and distribution is not sufficient for the MR fluid transition. Therefore, a larger piston with more windings and different coil winding direction is chosen.
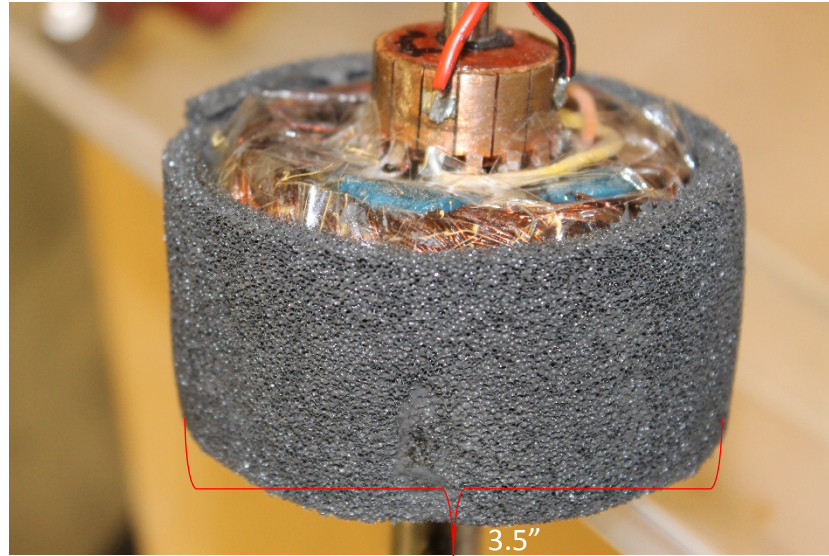
Figure 4.4 Piston with MR fluid sponge and electromagnet

The picture of the piston incorporating the electromagnet and wrapped up with Polyurethane foam is shown in Figure 4.4. The polyurethane foam is soaked with MR fluid and acts as MR fluid reservoir.

4.1   Fabrication of the MR Device

The initial design of the damper is made with the following dimensions as shown in Table 4.1. The coil is wound in the piston gap and tested for the desired magnetic field using a Gauss meter shown in Figure 4.5.

The magnetic field recorded is 0.5T, which is too small for the transition to take place in MR fluid. Therefore, a better design with increased dimensions in all the components is developed. The dimensions of the piston model is shown in the Table 4.1. The Table 4.2 shows final design of the device and Figure 4.6, 4.7 show the electromagnet with polyurethane foam. The material selected for the piston and cylinder is a low carbon steel to reduce the effect of flux leakage in the magnetic circuit of the electromagnet.

Figure 4.5 Gauss meter with probe for magnetic field detection
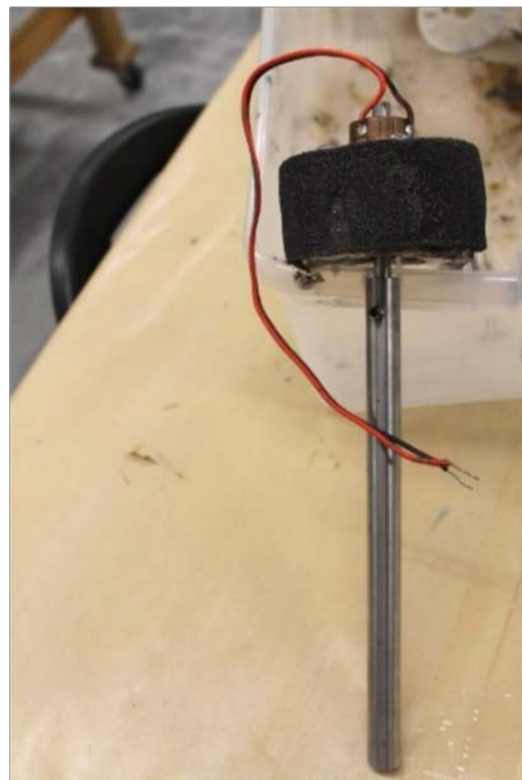
Figure 4.6 MR damper piston with electromagnet and sponge
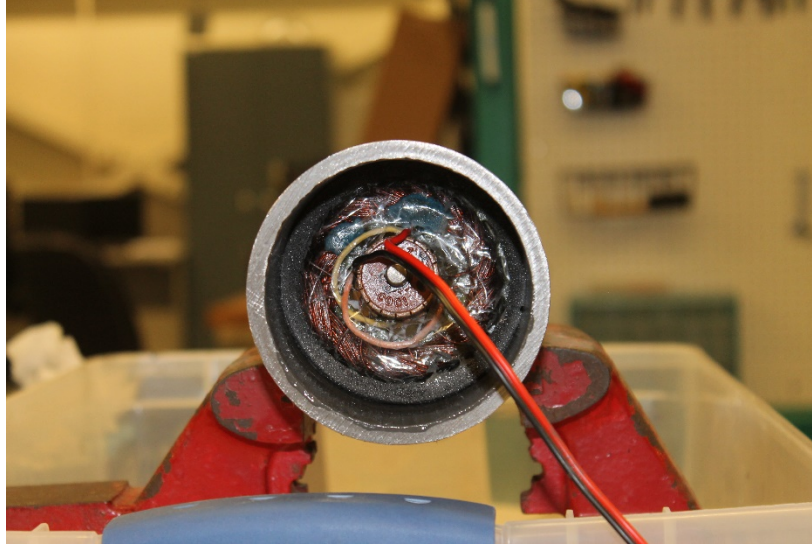
Figure 4.7 Front view of MR damper with piston inside the cylinder

Table 4.1 Preliminary MR damper parts with dimensions

No	Components	Dimensions
1.	Piston diameter	1in
2.	Piston rod length	10in
3.	Gap length	0.5in
4.	Cylinder ID	1.25in
5.	Cylinder length	8in

Table 4.2 Final MR damper parts with dimensions

No	Parameter	Value
1.	Piston diameter	3.125 in
2.	Piston rod length	10 in
3.	Cylinder ID	3.5 in
4.	Cylinder OD	4 in
5.	Cylinder Length	7 in

4.2   Selection of Polyurethane (PU) foam

Gong, Wu, Gong, Fan, & Xia (2013) work on polyurethane foam is used as reference for material selection for the MR fluid reservoir. The paper explains about the material properties of polyurethane foam and different configurations of MR foam are also analyzed. The PU foam is a polymer with foam matrix and it has different cell structures based upon the absorbent matrix. For this specific application of feel force, an open celled polyurethane foam is selected.

To validate the selection of polyurethane foam as MR fluid reservoir, the absorbing capacity of the foam is tested in the laboratory. Two different foam materials are selected and their absorbing capacity are tested. The foam materials used here are open celled polyurethane foam and closed cell polyurethane foam. The density of closed cell PU foam used is 0.002 lb/in^3. The cell volume of the material is approximately 0.000492/in^3. This foam is shown as white colored sponge in Figure 4.8 below.

Figure 4.8 Closed cell PU foam sample

The yield strength of closed cell foam is 0.003 ksi. Another important parameter to study is the fatigue strength of the material, which is 0.0127 ksi at 10^7 cycles. The CES edupack

software is used to make the material selection between closed cell and open cell foam.

The density of the open celled PU foam is 0.002 lb/in^3 and the volume of the cell is 8.19e4 /in^3. The open celled PU foam is shown in Figure 4.9. It is clear that the cell size is larger in the open celled foam than the closed cell foam. The yield strength in open celled foam is same as that of closed cell one. But the fatigue strength of the open celled foam is 0.011 ksi for 10^7 cycles. Another important parameter is the water absorbing capacity of the foam which is 10-11% for 24 hours.

Figure 4.9 Open cell PU foam sample

To experiment the absorbing capacity of both the foam materials, two foam specimens are taken with equal dimensions 2 in×2 in×0.1 in. The initial weight of both the specimens are recorded and is shown in Figure 4.10 and 4.11. Equal quantity of MR fluid is poured into both the foam material and left for 24 hrs. After 24 hours, the loss of MR fluid from both the foam materials are monitored. This can be done by measuring the weight of the foam with MR fluid, so that the amount of leakage can be identified.
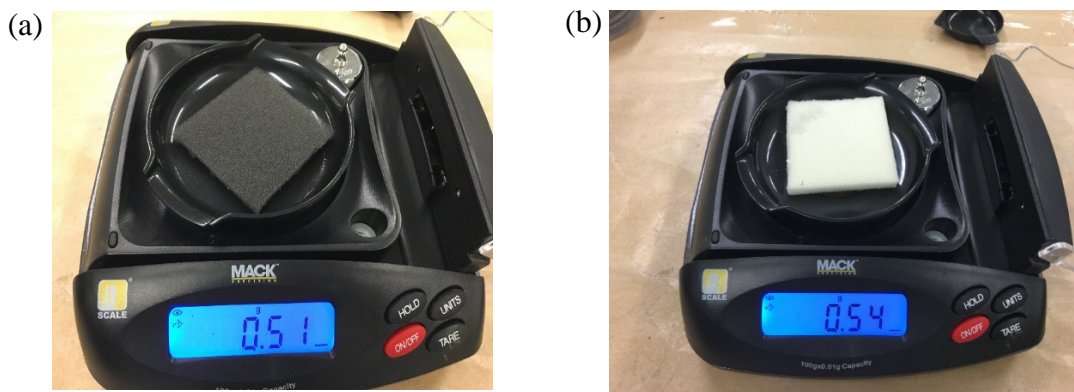
(a)

(b)

Figure 4.10 (a) Closed cell PU foam without MR fluid (b) Open cell PU foam with MR fluid

The weight of the closed cell foam is little higher than the open celled foam, however the experiment shows that the closed cell foam has more leakage of fluid than the open celled foam. This can be proven by monitoring the weight of the closed cell foam. The data about the weight of foam before and after 24 hours are shown in the below Table 4.3. Figures 4.11, 4.12 shows the weight of the foam materials before and after 24 hours.
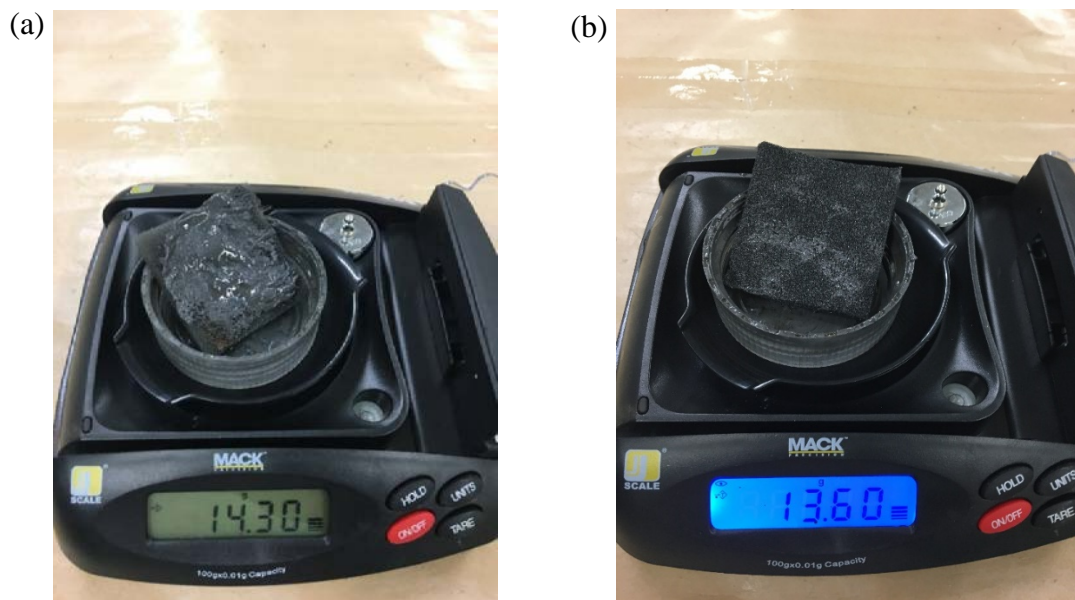
(a)

(b)

Figure 4.11 Weight of open cell PU foam with MR fluid (a) before 24 hours (b) after 24 hours

It can be seen from the picture that the open cell foam allowed only 0.70 g of MR fluid over 24 hours. Same procedure is followed for open celled foam material.
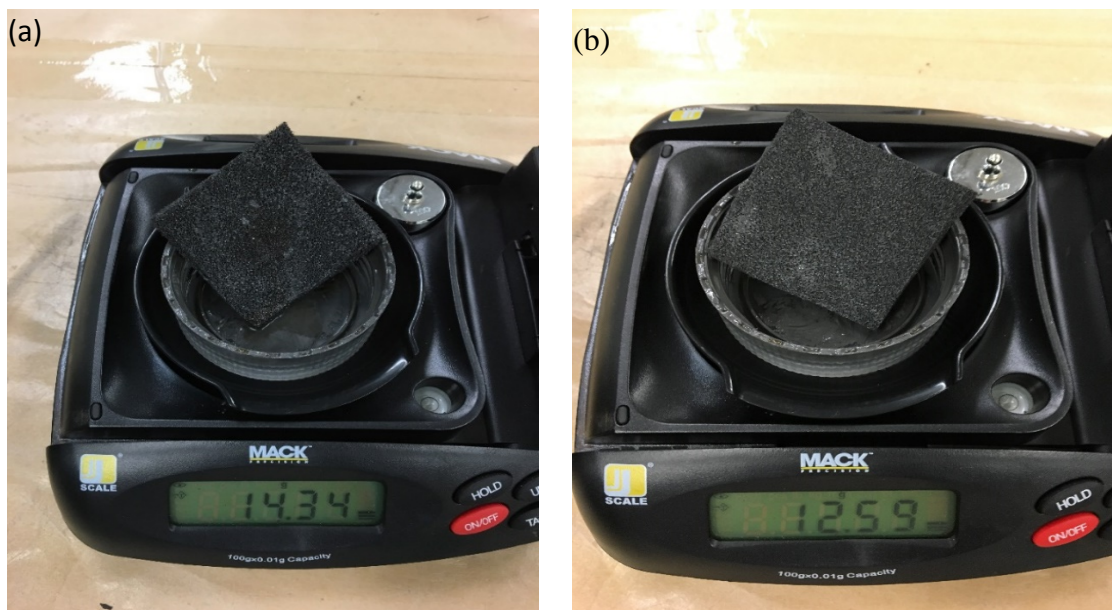

Figure 4.12 Weight of closed cell PU foam (a) before 24 hours (b) after 24 hours

Table 4.3 Weights of PU foam at different time

Material type	Weight without fluid (g)	Weight before 24 hours (g)	Weight after 24 hours (g)
Open cell	0.51	14.30	13.60
Closed cell	0.54	14.33	11.40

The primary advantage of using this open cell structure is the pore size and it ranges from 250-500 microns. The carbonyl particles from the carrier fluid of the MR fluid enters the porous structures and remains active inside the cell. This open cell structure improves the absorbing capacity of the foam and this is proved in the laboratory experiment.

The experimentation on absorbing capacity of polyurethane foam is done by Mohan, Hickman, Balakrishnan and Saha (2008). The experimental procedure from the paper is used in validating the open celled PU foam mechanical properties. The material is also very light and the thickness of the foam is 0.1in and it is compressed in the inner side of the cylinder. The durability of foam is very high and the material can withstand larger number of working cycles than other foam materials.

5. Magneto-Static Analysis

After the preliminary design of the damper is developed, it is analyzed for the magnetic field distribution using ANSYS APDL. The specific design of the damper is developed as an axisymmetric model and the magneto-static analysis is performed. The axisymmetric design is shown in Figure 5.1.

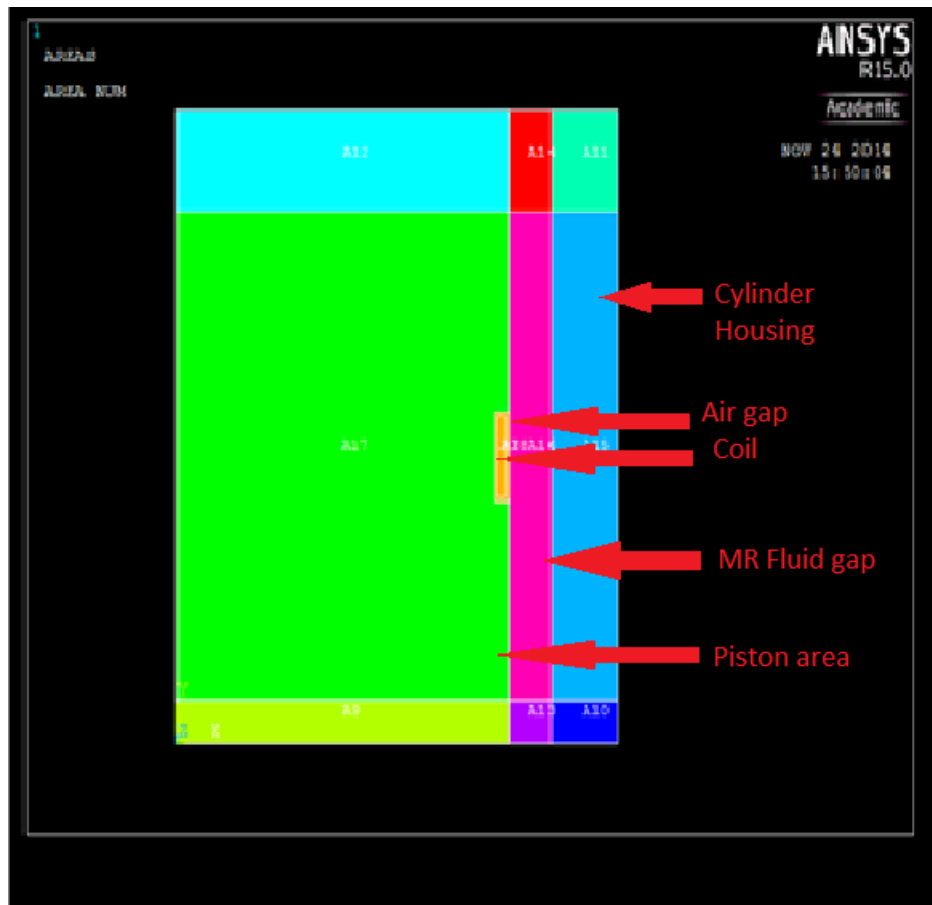Figure 5.1 Axisymmetric model of MR damper created in ANSYS

This axisymmetric model is developed based on the first design of the piston and cylinder. The model is developed in ANSYS and all the areas of the model are made concurrent which can be seen with different colors in Figure 5.1. The green area represents the symmetric cut section of the piston. The area with blue color represents the cylinder

wall. The coil section in the piston is shown as orange color area. The air gap is an area between the coil and the MR fluid section. The dimensions of the area used in the axisymmetric modeling is shown in Table 5.1

Table 5.1 Area dimensions of different components of MR damper developed in ANSYS

No	Component	Area (l*b)
1.	Piston	3in×2in
2.	Coil gap	0.5in×0.02in
3.	MR fluid gap	3in×0.3in
4.	Cylinder housing	3in×0.5in

El-Aouar, Walid (2002) did research in finite element modeling of MR damper piston. Their research explains the importance of piston design in the MR damper. Ferdaus, Mohammad (2014) discusses the different configurations of MR damper piston to achieve maximum magnetic field distribution with optimized design of the piston. The analysis procedure followed by El-Aouar, Walid (2002) is used in performing magneto static analyses for the feel system application.

Figure 5.2 below shows the mesh region developed for different components of the piston and cylinder in the entire assembly. The meshing is created with 4 different regions and same element size. The input parameter for the FEA model is current density and is specified as 2 A/m^2. The relationship between magnetic field B and flux density can be obtained from the "Shock absorber handbook" by Dixon (2008). The book explains some of the physical properties of MR fluid such as permeability constant.
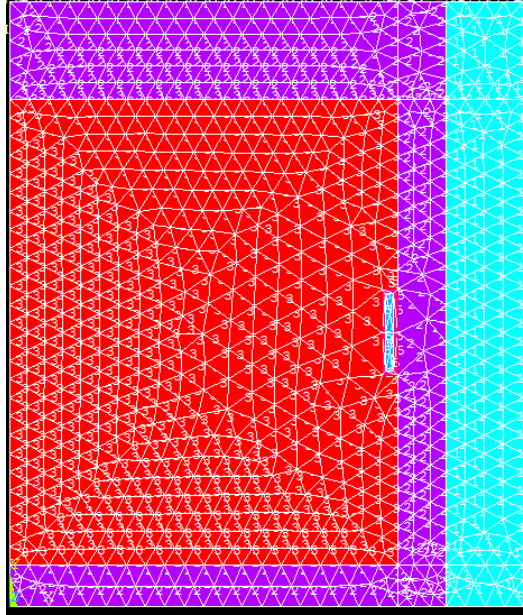
Figure 5.2 Mesh model created for MR damper with 4 different regions

The BH curve for the input current is manually chosen and given as input as shown in Table 5.2 and Figure 5.3 shows the BH curve.

Table 5.2 BH curve data points

No.	B (T)	H (A/m)
1.	0.24	35
2.	0.40	70
3.	0.49	155
4.	0.56	320
5.	0.60	630

For this current density and with specific piston design, the magnetic vector lines obtained is shown in Figure 5.4. From the vector lines result, it is clear that the magnetic field is concentrated in only specific region, which is shown in red color lines.
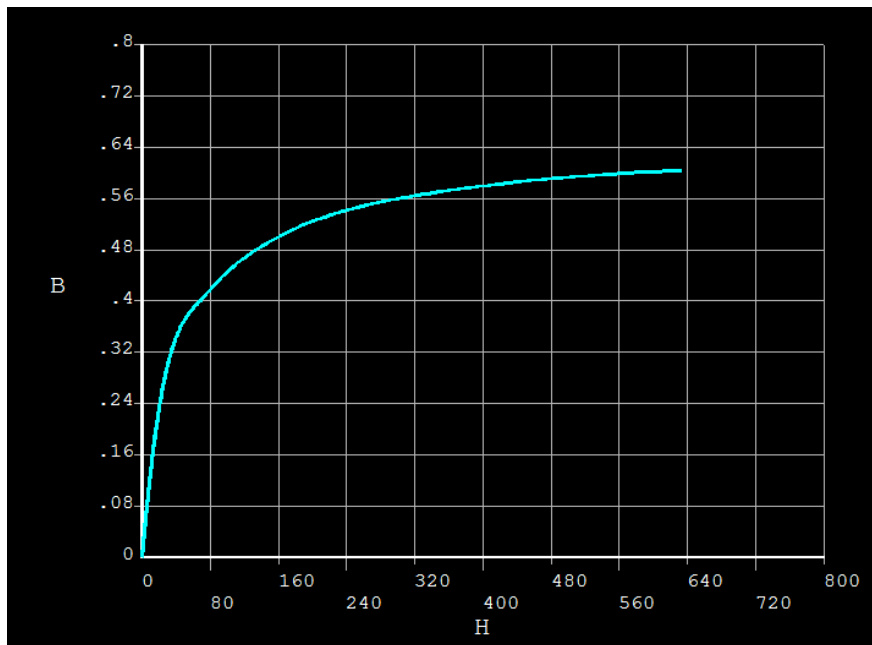
Figure 5.3 BH curve generated in ANSYS APDL

Even though the magnetic field is closely narrowed in the MR fluid region, the strength is not enough to generate required force. Therefore, the piston design and coil winding gap is altered for greater magnetic field strength.
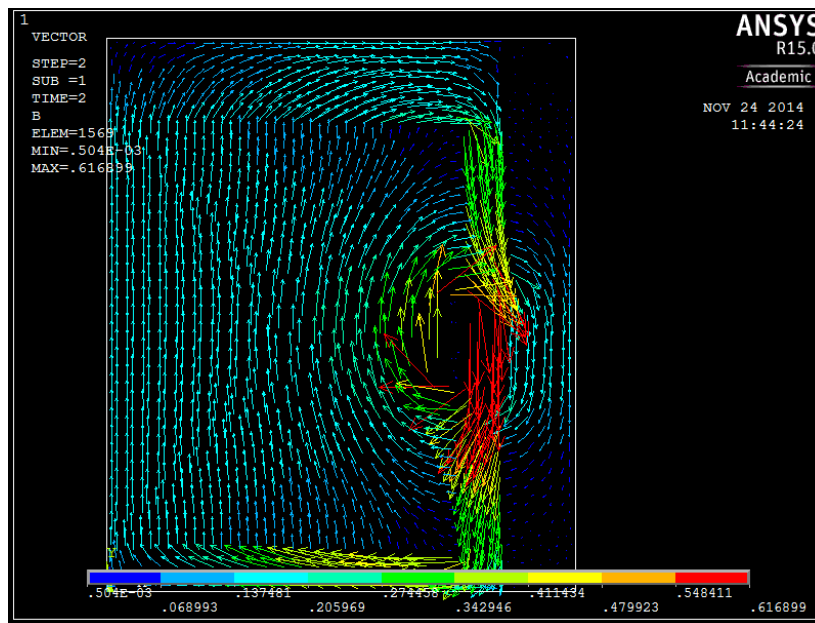

Figure 5.4 Magnetic vector lines with magnetic field intensity

6. MR Damper Testing

The fabricated damper is tested for checking its functionality at this phase of research. The damper is tested using Universal Testing Machine for compression and tension tests.

The MR device is fabricated as a simple piston and cylinder assembly. The fabricated device is tested for the force-velocity characteristics using a tensile/compression testing machine (MTS machine) available in the aerospace structures lab at Embry-Riddle University. The MTS machine has the load testing range of 10,000 lb. The testing is performed to check the compatibility of MR device with the foam design for specific application. The device is mounted on the MTS machine with the cylinder on top and piston attached to the bottom clamp. The upper end grip of the machine is fixed and stationary, while the lower end grip is attached to a movable shaft that enables displacement of the MR device piston. The power supply for the electromagnet inside the piston is setup and it is remotely controlled using LabVIEW software.

A LabVIEW code is developed to input current to the electromagnet through NI-DAQ. The mounting of MR device onto the MTS machine is shown in Figure 6.1. The resultant forces are plotted for velocity and displacement from the MTS machine and are shown in Figures 6.2 and 6.3 respectively.
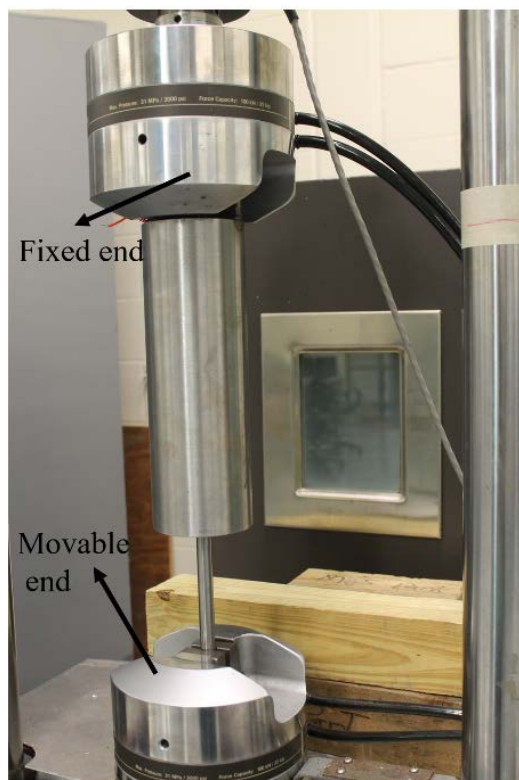
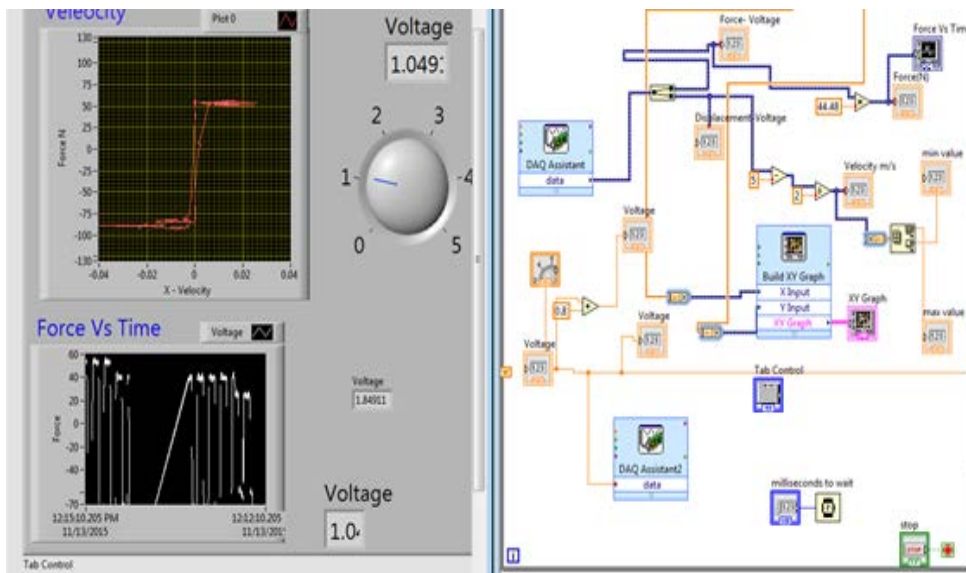Figure 6.1 MTS machine with MR damper mounted on the clamps

Figure 6.2 LabVIEW code with front panel and block diagram with velocity output
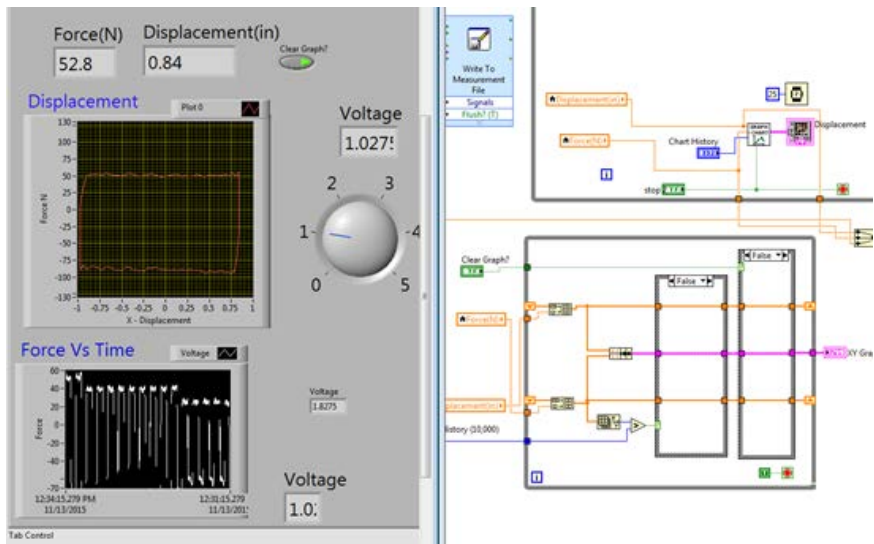
Figure 6.3 LabVIEW code with block diagram and front panel with displacement output

6.1   NI myDAQ

The NImyDAQ is a data acquisition card for real time data analysis and processing. It has 2 analog input, 1 analog output and 8 digital input terminals. It is powered by USB cable and can be easily interfaced with any computer. The operating range for sensor inputs and outputs from the DAQ is 5V.
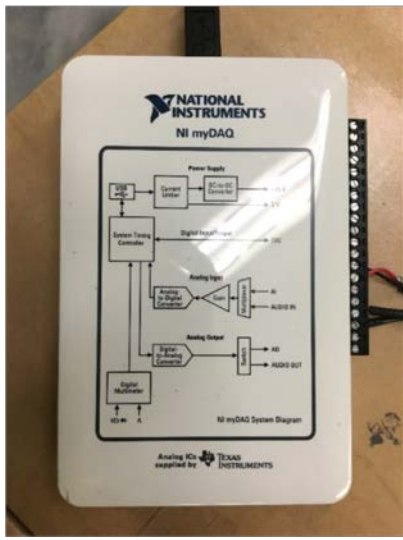

Figure 6.4 NImyDAQ with wires connected to the output terminal

6.2   Experiment

Different current values are selected and given as inputs to the device and the corresponding force-velocity characteristics are recorded. The experiment is started with 2A of current and the force is recorded approximately as 10 N. The maximum current that can be supplied to the device is recorded as 17A. However, the required force of 70 N is achieved for 14A current and therefore 14A is set as current saturation limit for the device. The response time of the device for each change in input current is also recorded. For 5A current, the device recorded 25 N of force and also from the previous current values, it is clear that the force from the device relatively increase or decrease based on relative change in current values. The experimentation of MR damper using DAQ system and remotely controlled power supply is shown in Figure 6.5.
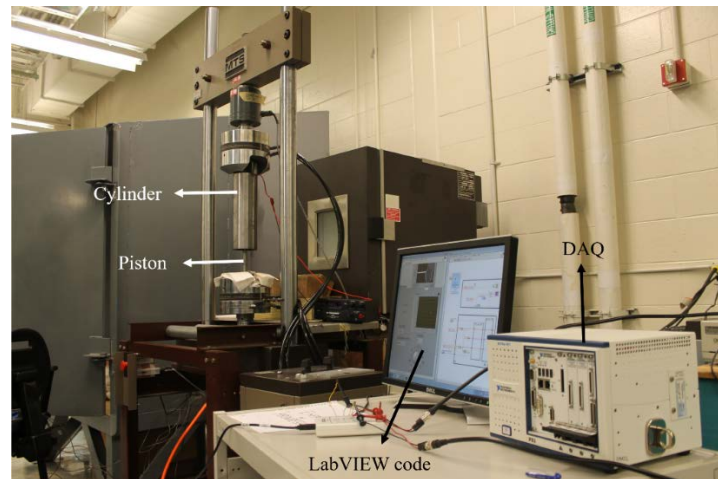

Figure 6.5 MR damper connected with external power supply and DAQ system

6.3   Experimental result

The force vs velocity plot shown in Figure 6.7 provides sufficient details about the constructed MR device. The pattern of the plot closely follows the traditional Bingham plastic model as the force range is constant for different velocity values. However, the

device shows hysteresis in the experimental result which is neglected in the mathematical model, compromising the accuracy for an easier modeling method. The current values are randomly chosen with the first value being 2.2A and the corresponding forces are plotted against velocity. For instance, comparing the displacement and velocity plot for the 5A current, the device provides 25 N of force approximately. The uneven lines in the plot are due to noise and other disturbances in data acquisition and also errors from the MTS machine itself. With proper noise filtering, the disturbances in data acquisition can be reduced and better results can be recorded. The experiment is performed for particular number of cycles to validate the device performance.

The device recorded a maximum of 70 N in positive direction and 100 N in negative direction for an input current of approximately 14A. The different range of forces in positive and negative directions are due to the minor misalignment of piston and cylinder when mounted in the MTS machine. The error is also due to non-uniformity of the cylinder inner diameter due to minor imperfections. This error can be avoided by using a precisely fabricated steel cylinder which could demand a high fabrication cost. The maximum force recorded in the positive direction can be considered as the maximum force offered by the device. The results prove that the device is capable of providing 70 N of force which also meets the FAA standards for force on control stick (FAA standards for control forces, 2016).

Based upon the future applications and further requirements, different experimentation procedures can be followed to test the device for various applications. For example, durability test can be performed to test the device for force characteristics in a particular number of cycles. Failure tests can be performed to estimate possible means of

device failure. Saturation tests can be performed to check the capacity of the device for current input, as the device cannot supply more force after it reaches the saturation limit for the specific current value. The results from the experiment are shown in Figure 6.6 and 6.7. Further results can be gathered from the appendix A section.
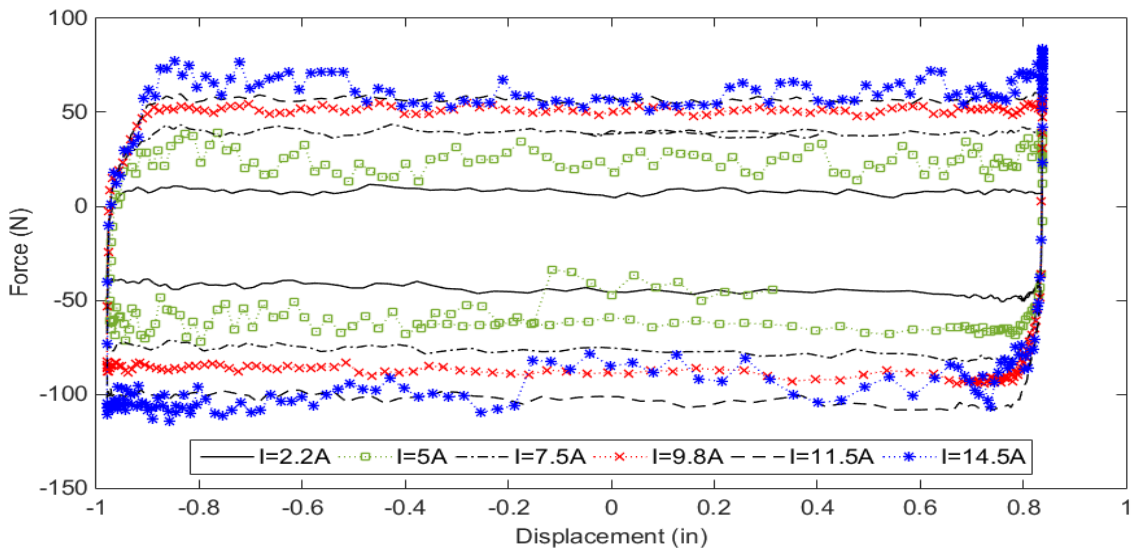

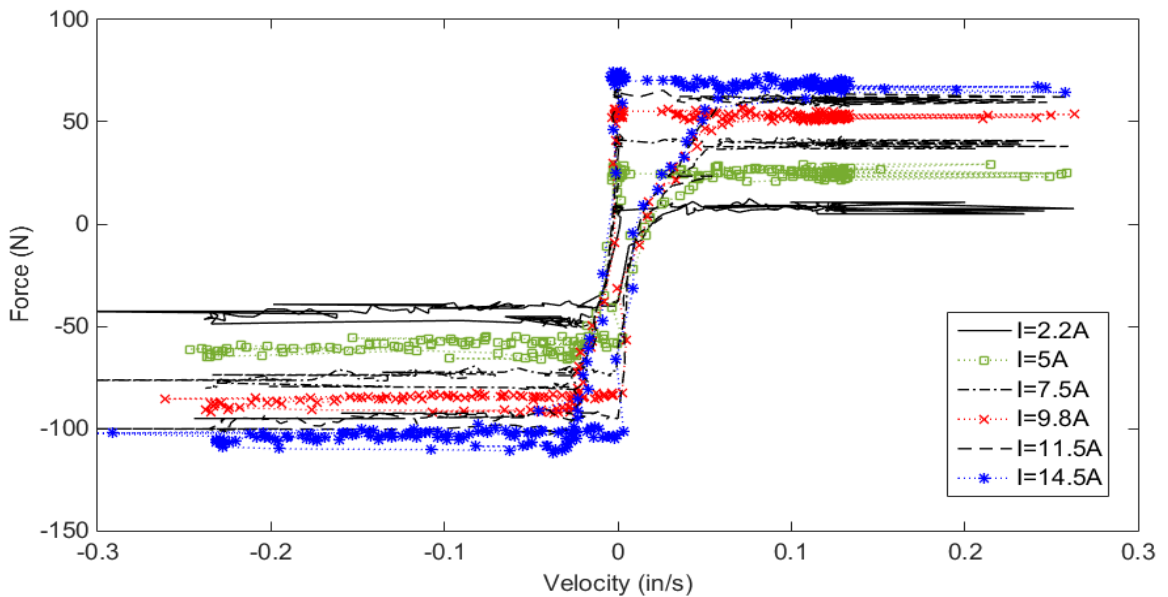Figure 6.6 Experimental force vs displacement graph of MR damper

Figure 6.7 Experimental force vs velocity plot of MR damper

7. MR Device Model Simulation

After testing the functionality of the MR device, validation of the derived mathematical model for the MR device is performed. The derived transfer function model is a multi-input single output system. The mathematical model is simulated using LabVIEW software and control simulation loop is used to perform the simulation. Later, the final transfer function equation is used as input blocks in LabVIEW software. Also, different blocks are constructed and combined into the simulation model using mathematical operator in the software. The coefficients, such as b_H, k_H, T_e and T_m that are used in the transfer function equation, are experimentally found and also acquired from the work of Milecki. In the simulation model, the velocity and voltages are given as inputs and the force is obtained as output.

The first transfer function block converts the given voltage into current value. The input current is saturated in the next block and given to the second transfer function. The given input current is changed into the corresponding shear stress based on the magnetic field function in this block. The velocity in simulation is given as a constant value and also a constant viscosity gain of 1 is selected. The output is monitored in a graph and the corresponding values are recorded.

The simulation loop in LabVIEW software is shown in the Figure 7.1. The simulation is performed with the same set of current values used for experimentation so that it will be easy to compare the experiment with the simulation result. Only the velocity plot is acquired for the simulation as it is sufficient enough to prove the certainty of the derived mathematical model. The velocity plot also follows the same traditional Bingham plastic model pattern. The force remains constant for different velocity range.
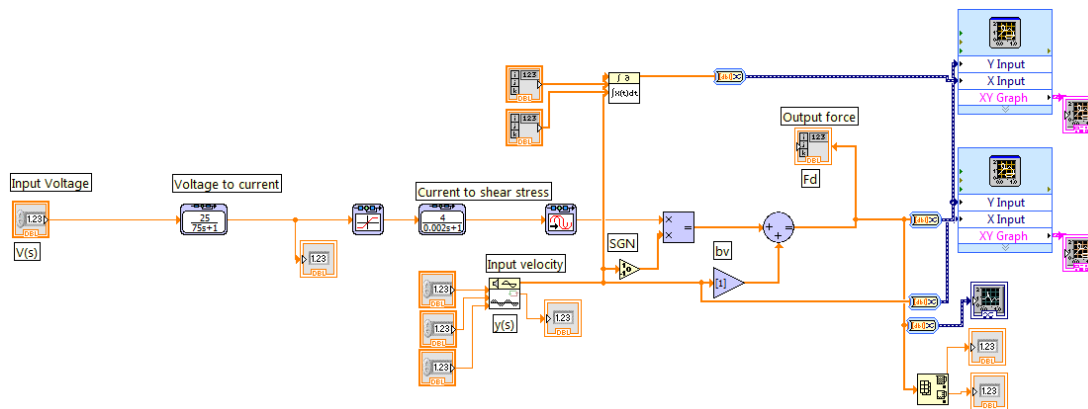
Figure 7.1 Simulation loop created in LabVIEW with transfer function blocks

7.1 Simulation result

The comparison of simulation and experimental model is done to validate the certainty of using Bingham model for this specific application. It is found from the simulation that the force ranges are equally distributed in both directions. The maximum force recorded in the simulation model is 60 N for current of 14.5 A. The maximum force recorded in the experimental model for the same 14.5 A is approximately 75 N. The force from the positive direction is used for comparison due to close range of force with simulation model.
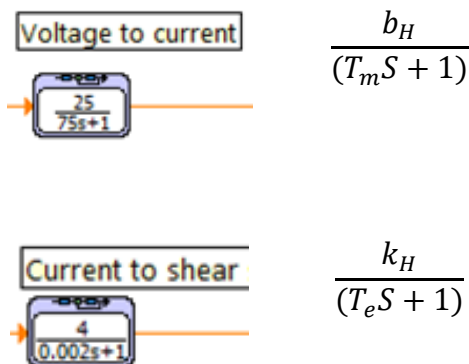

Figure 7.2 Transfer function blocks with mathematically developed transfer function

Since this is a mathematical model, there are no possible noise errors and the lines on the force-velocity plots are straight. The hysteresis parameter is not included in the mathematical model and hence the force lines in the simulation force-velocity plot are vertically straight. But hysteresis is present in the real time force-velocity experimentation plot and this is one of the result that can be improved in the future by choosing better mathematical modeling approach. The accuracy of the model can be improved by including the hysteresis and also friction characteristics of the MR device in the model. The transfer function equation from the mathematical model is used as transfer function blocks in LabVIEW and it is shown in Figure 7.2. Figure 7.3 shows that the experimental and simulation results are in close range for the same current input values.
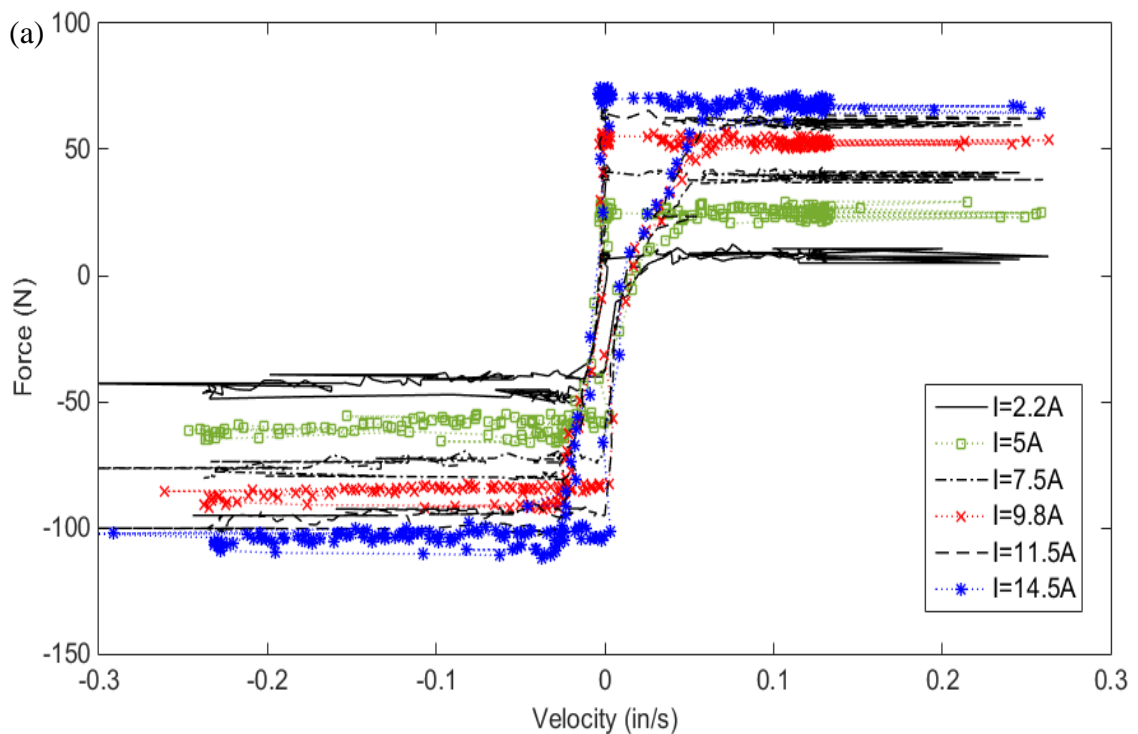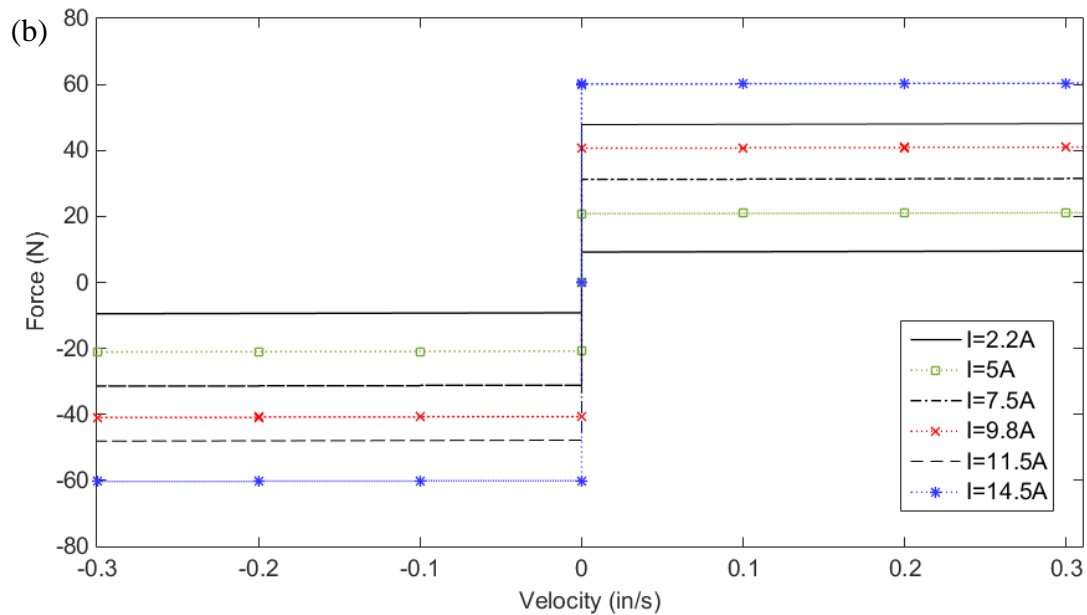
Figure 7.3 Comparison of Force vs velocity plot of experiment and simulation (a) experimental, (b) simulation

8. System Development and Testing

The assumptions made for mathematical modeling of the MR device replicates the mechanical characteristics of the device and it is proved from the simulation. The development of artificial feel system is carried out after the experimentation and simulation of the MR model.

To replicate the real time control stick, a Logitech flight simulator joystick is used. For simplicity purpose, the pitch control (Y axis) motion of the joystick alone is used for feel force application.
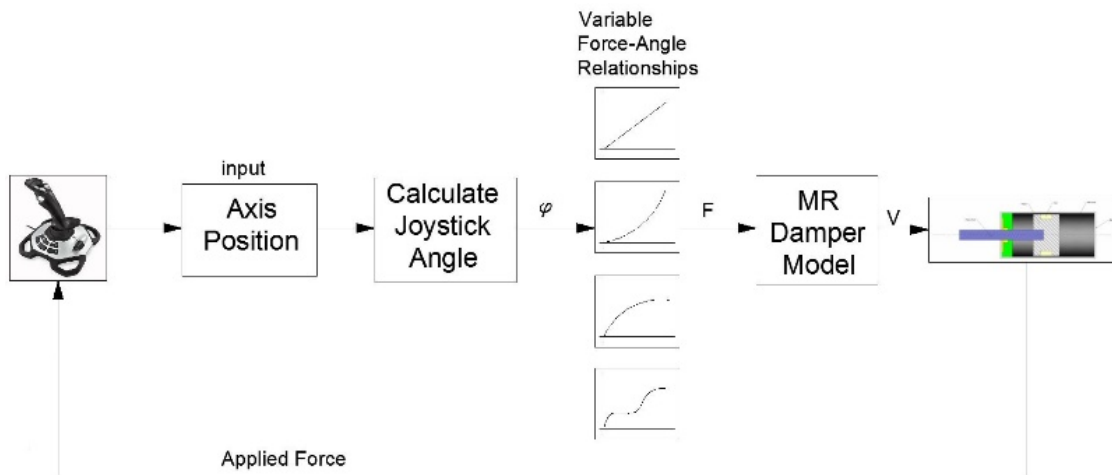

Figure 8.1 Functional flow diagram of joystick integration with LabVIEW

The joystick is considered as pilot's control stick and it is interfaced with the MR device piston and the piston has stroke length of ±2 inch. The block diagram for joystick integration and the program flow is shown in Figure 8.1.

8.1   Real time data acquisition

For the real time data acquisition, a load cell and laser displacement sensor is used. The load cell is interfaced between the piston and the joystick. The load cell is first calibrated with dead weights and corresponding voltage values are recorded for the force values. The load cell in the system is capable of measuring forces up to 250 N. The load cell is excited using an external power supply. Figure 8.2 shows the laboratory setup of the feel system. The laser displacement sensor monitors the velocity of the MR device piston. The load cell measures the force and gives as input parameter to the LabVIEW program. The input force is monitored and corresponding output voltage values are calculated and given as output to the MR device.
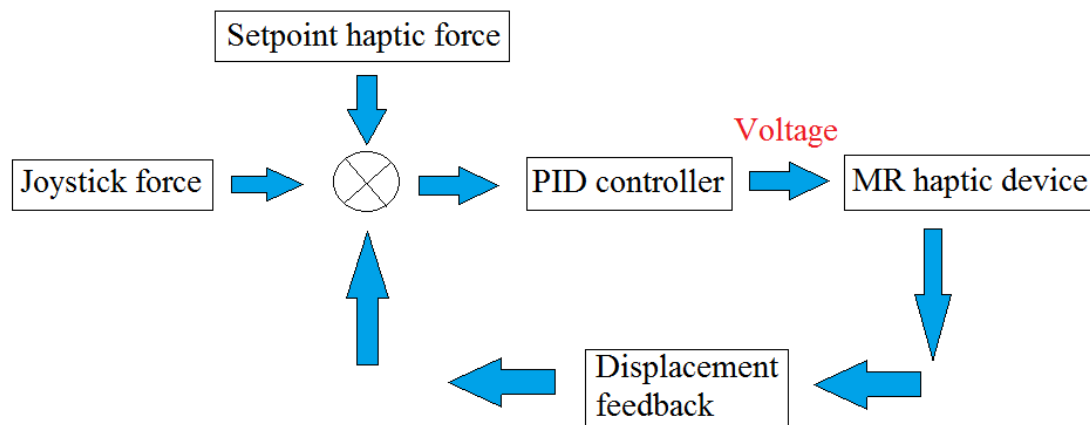
8.2   Force-feedback control

Figure 8.2 PID control loop block diagram for feel system

The block diagram for PID control operation in this research is shown in Figure 8.2. The PID control in the LabVIEW software is virtually created and the controller is tested in the software. This provides the advantage of testing the system for different gain parameters to achieve quick response time of the haptic device. The PID controller

continuously calculates the error between the setpoint variable and the measured process variable.

Sigurd Skogestad (2001) work on tuning of control loop is studied. This paper discusses about the novel techniques in tuning the gain parameters to achieve quick settling time. The paper conveys information about each proportional, integral and the derivative gains. The proportional gain should be high, integral gain should be less and the derivative gain should be high to get faster control of the system. The paper describes about different control techniques that can be achieved using different tuning approaches. It is concluded in the paper that Zeigler Nichols tuning method is the commonly used and good tuning methodology for PID controller.

Shahrokhi & Zomorrodi (2013) published a paper on comparing different tuning methodologies for PID controller. The tuning methodology is proposed only for SISO system and the integral of absolute error algorithm is used. The review is made using software and the different tuning methodologies are validated. However, the developed feel system is a MISO system and tuning methodologies are same for both MISO and SISO system.

Haugen (2010) conducted a review on tuning of PID control loop experimentally using temperature control system. This paper focuses more on tuning PI controller using performance of setpoint tracking and concludes the best approach to quickly tune any controller. A simple air heater experimental setup is created and the voltage supply to the heater is controlled. The NI LabVIEW is used to perform control operation. The block diagram for the PID control is shown in the below Figure 8.3. By considering the open loop and closed loop control operations for different methodologies, the indices of setpoint

tracking, disturbance compensation, and instability calculations are made. The paper concludes that Skogestad's method is the quickest and best methodology to tune the PI control loop for temperature control.
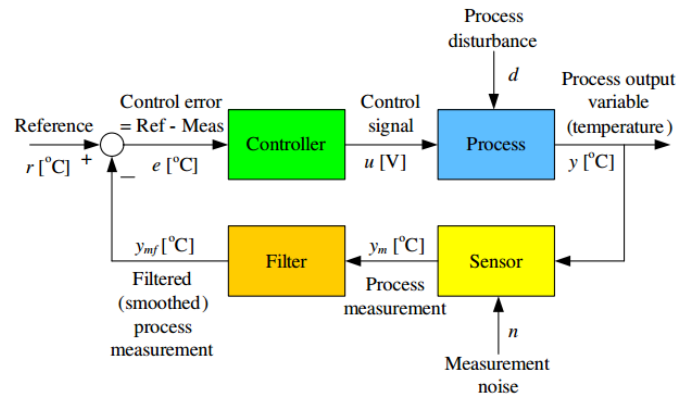

Figure 8.3 PID block diagram for temperature control system (Haugen, 2010)

Li, Liu, Kosasih & Zhang (2007) developed a force feedback system for 2 axis joystick using MR fluid device. The haptic device used in the above research provides force in both the X, Y directions by using LabVIEW software. The MR joystick in this research is proposed to be used in virtual reality application. The technical details used are followed to build a PID control loop for feel system and the feedback forces are automatically calculated based on the user input.

The experimental setup of the artificial feel system is shown in Figure 8.4. The input from the laser displacement sensor is given to the PID control loop. The desired output force value is given as set point to the PID loop. The NI DAQ hardware is used to interface the sensors with the LabVIEW program. After interfacing the sensors, the functionality of the entire system is tested. The response time and sampling rate of the device are monitored and adjusted based on the user requirement for the future work. The tuning techniques for the open loop and closed loop control systems are studied in detail and can be further implemented in optimizing the response time. By experimenting the

system with different tuning techniques in the PID control different response time can be achieved in the future.
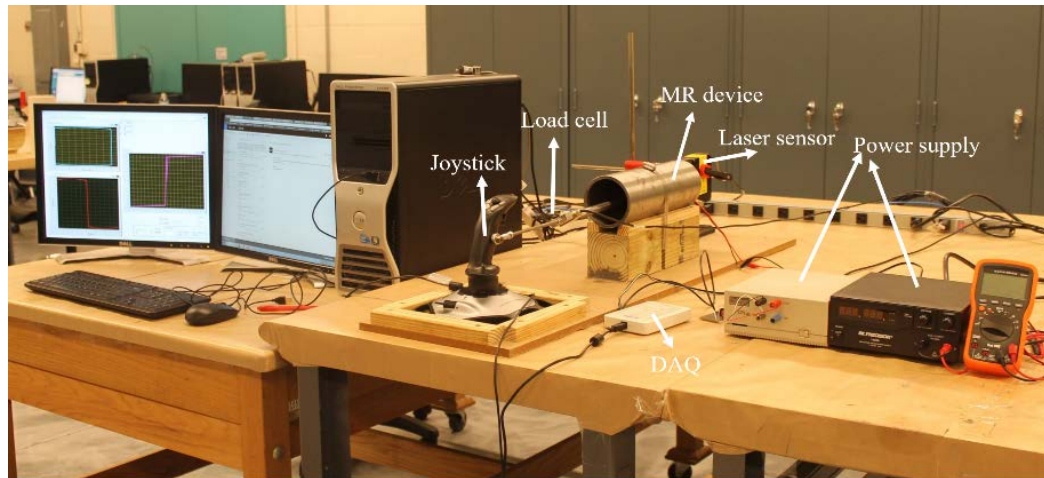

Figure 8.4 Laboratory setup of feel system with MR device and sensors interfaced

9. Conclusions and Future Work

The concept of using a MR fluid device in providing the feel force to the aircraft control stick is validated. The novel idea is modelled, simulated, experimented and analyzed for the specific aerospace application. In every stage of research, the device is proved to be compatible for feel force application. Significantly, the MR feel system is identified as compact, simple in construction, easy to interface with flight system, and offers precise control with high durability. These advantages of the system fulfill the objective of this research for smart feel system application applied to the aircraft control stick.

However, for the future work, better correlation between simulation and mathematical model can be achieved by using an improved MR model such as Bouc-wen model. Further improvement in the experimental results can be made by using more precisely machined cylinder with less imperfection in inner diameter. For the installation of the device into real time cockpit of aircraft, the weight of system must be reduced. Therefore, a unique design using 3D printed cylinder using plastic material and having steel lining inside the cylinder is proposed. The device can be further examined based on industry standards for commercialization in the future.

REFERENCES

Ahmadkhanlou, F., Mahboob, M., Bechtel, S., and Washington, G. (2012). "An Improved Model for Magnetorheological Fluid-Based Actuators and Sensors," Journal of Intelligent Material Systems and Structures, 21, 3-18.

Ahmadian, M., & Poynor, J. C. (2001). An evaluation of magneto rheological dampers for controlling gun recoil dynamics. Shock and Vibration, 8(3-4), 147-155.

"Artificial feel system" (19 January 2016) retrieved from https://www.quora.com/How-does-the-control-joystick-in-Airbus-aircraft-work

Avraam, M., & Preumont, A. (2009). MR-fluid brake design and its application to a portable muscular device.

Berthet, J.-L. and Bondivenne, E. (1998)., "Control Device with a Control Stick, Particularly a Servo Sidestick for Aircraft," U.S. Patent No. 5,735,490.

Bingham, E. C. (1922). "Fluidity and Plasticity", New York: McGraw-Hill.

Braz Cesar, M., and Carneiro de Barros, R. (2012). "Properties and Numerical Modeling of MR dampers," 15th International Conference on Experimental Mechanics, Porto, Portugal, 4050.

Bucchi, F., Forte, P., Frendo, F., & Squarcini, R. (2013). A magnetorheological clutch for efficient automotive auxiliary device actuation. Frattura ed Integrita Strutturale, (23), 62.

Butz, T., and O. Von Stryk. (2002). "Modelling and simulation of electro-and magnetorheological fluid dampers." *ZAMM* 82.1: 3.

Carlson, J. D., & Jolly, M. R. (2000). MR fluid, foam and elastomer devices. mechatronics, 10(4), 555-569.

Chrzan, Michael J., and J. David Carlson. (2001). "MR fluid sponge devices and their use in vibration control of washing machines." SPIE's 8th Annual International Symposium on Smart Structures and Materials. International Society for Optics and Photonics.

"Cyberbond Apollo2025, (20 January 2016)."http://www.cyberbond1.com/productdetail/apollo/2025.

Deng, H. X., Gong, X. L., & Wang, L. H. (2006). Development of an adaptive tuned vibration absorber with magnetorheological elastomer. Smart materials and structures, 15(5), N111.

Dixon, John. (2008). "The shock absorber handbook". John Wiley & Sons.

El-Aouar, Walid H. (2002). "Finite element analysis based modeling of magneto rheological dampers". Diss. Virginia Polytechnic Institute and State University.

"FAA standards for control forces" (25 January 2016). Referred from http://flighttraining.aopa.org/students/presolo/topics/controlforces.html.

Ferdaus, Mohammad Meftahul, (2014). "Optimal design of Magneto-Rheological damper comparing different configurations by finite element analysis." Journal of mechanical science and technology 28.9: 3667-3677.

Gavin, H., Hoagg, J., and Dobossy, M. (2001). "Optimal Design of MR Dampers," U.S.-Japan Workshop on Smart Structures for Improved Seismic Performance in Urban Regions, Seattle, WA, 225-236.

Gong, Q., Wu, J., Gong, X., Fan, Y., & Xia, H. (2013). "Smart polyurethane foam with magnetic field controlled modulus and anisotropic compression property". RSC Advances, 3(10), 3241-3248.

Griffith, C. (1978). "Fail Safe Force Feel System," U.S. Patent No. 4,106,728.

Grunwald, A., & Olabi, A. G. (2008). Design of magneto-rheological (MR) valve. Sensors and Actuators A: Physical, 148(1), 211-223.

Hanlon, C., Potter, C., and Wingett, P. (2011). "Active Control Stick Assembly," U.S. Patent No. 8,056,432.

Harwood, Kenny, (2011). "Modeling a RLC Circuit's Current with Differential Equations," FVCC.

Haugen, F. (2010). Comparing PI tuning methods in a real benchmark temperature control system. Modeling, Identification and control, 31(3), 79.

Li, W. H., Liu, B., Kosasih, P. B., & Zhang, X. Z. (2007). "A 2-DOF MR actuator joystick for virtual reality applications". Sensors and Actuators A: Physical,137(2), 308-320.

Liu, B., Li, W. H., Kosasih, P. B., & Zhang, X. Z. (2006). Development of an MR-brake-based haptic device. Smart Materials and Structures, 15(6), 1960.

Maślanka, Marcin, Bogdan Sapiński, and Jacek Snamina. (2007). "Experimental study of vibration control of a cable with an attached MR damper." Journal of Theoretical and Applied Mechanics 45.4: 893-917.

Milecki, Andrzej, and Mikołaj Hauke. (2012). "Application of magnetorheological fluid in industrial shock absorbers." Mechanical Systems and Signal Processing28

Milecki, Andrzej, (2001). "Investigation and Control of Magneto–rheological Fluid Dampers," International Journal of Machine Tools and Manufacture, 41(3), 379-391.

Neelakantan, Vijay A., Gregory N. Washington, and Randall K. Wolf. (2002). "Force feedback system using magneto-rheological fluids for telerobotic surgery."SPIE's 9th Annual International Symposium on Smart Structures and Materials. International Society for Optics and Photonics.

Poynor, James C. (2001). "Innovative designs for magneto-rheological dampers". Diss. Virginia Polytechnic Institute and State University.

Sapiński, B., Snamina, J., Maślanka, M., & Rosół, M. (2006). "Facility for testing of magnetorheological damping systems for cable vibrations". Mechanics/AGH University of Science and Technology, *25*, 135-142.

Shahrokhi, M., & Zomorrodi, A. (2013). Comparison of PID controller tuning methods. Department of Chemical & Petroleum Engineering Sharif University of Technology.

Sigurd, S. (2001). Probably the best simple PID tuning rules in the world. Journal of Process Control.

S. Mohan, D.L. Hickman, A. Balakrishnan, and M. C. Saha, (2008)."Effect of Moisture Absorption Characteristics on Flexure Properties of Polyurethane Foams," Twenty Eight AIAA/ASME Symposium, Oral Roberts University, Tulsa, Oklahoma.

"Smart Materials," (19 January 2016). Retrieved from https://webdocs.cs.ualberta.ca/~database/MEMS/sma_mems/smrt.html.

Spencer, B. F., Dyke, S. J., Sain, M. K., & Carlson, J. (1997). Phenomenological model for magnetorheological dampers. Journal of engineering mechanics, 123(3), 230-238.

Symans, M. D., & Constantinou, M. C. (1999). Semi-active control systems for seismic protection of structures: a state-of-the-art review. Engineering structures, 21(6), 469-487.

Talatahari, S., & Rahbari, N. M. (2015). Enriched Imperialist Competitive Algorithm for system identification of magneto-rheological dampers. Mechanical Systems and Signal Processing, 62, 506-516.

Truong, D. Q., and Ahn, K. K. (2012). "MR Fluid Damper and its Application to Force Sensorless Damping Control System," INTECH Open Access Publisher.

Tu, F., Yang, Q., He, C., & Wang, L. (2012). Experimental study and design on automobile suspension made of magneto-rheological damper. Energy Procedia, 16, 417-425.

Wang, Yingru. (2006). "Modeling of polymer melt/nanoparticle composites and magneto-rheological fluids". Diss. The Ohio State University.

Zhu, C. (2005). A disk-type magneto-rheological fluid damper for rotor system vibration control. Journal of sound and vibration, 283(3), 1051-1069.

A. Appendix-LabVIEW Code for the MR Damper experiment

The LabVIEW program for the MR damper tensile and compression test with different voltage range values and force vs velocity plots are shown in Figure 10.1 to Figure 10.6 below.
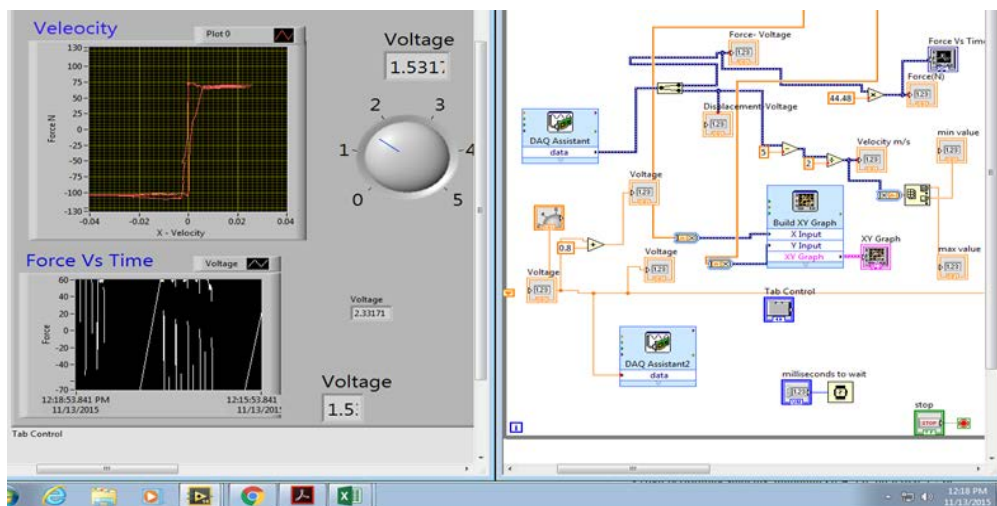
Figure 10.1 Force vs velocity plot for 1.53V
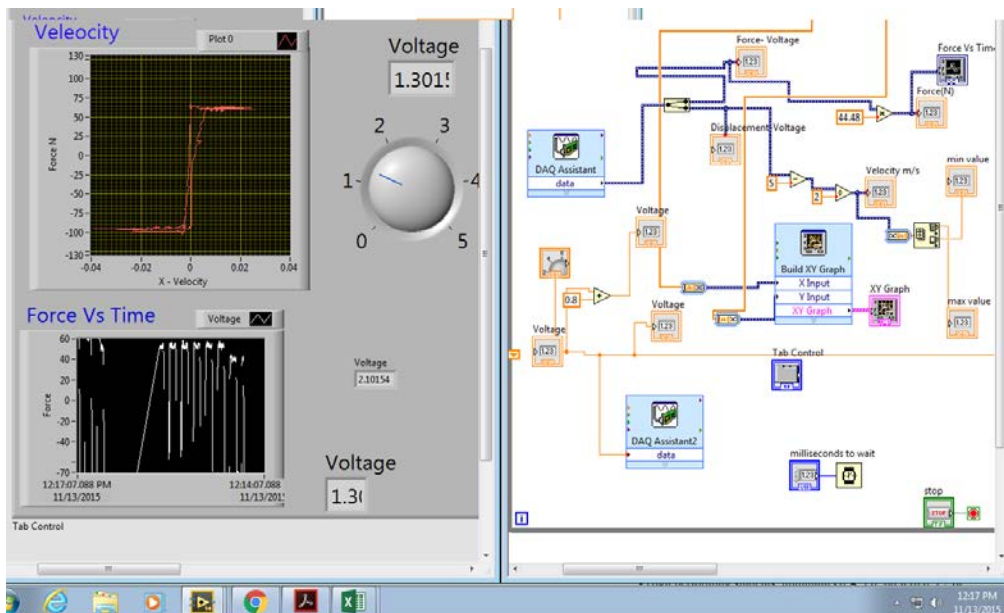
Figure 10.2 Force vs velocity plot for 1.3V
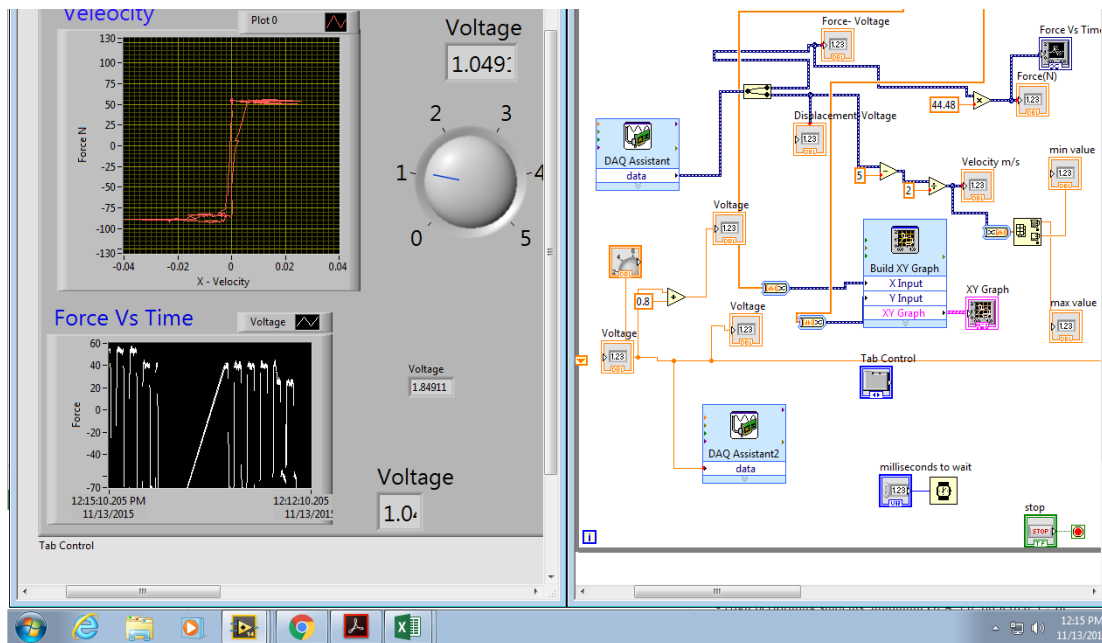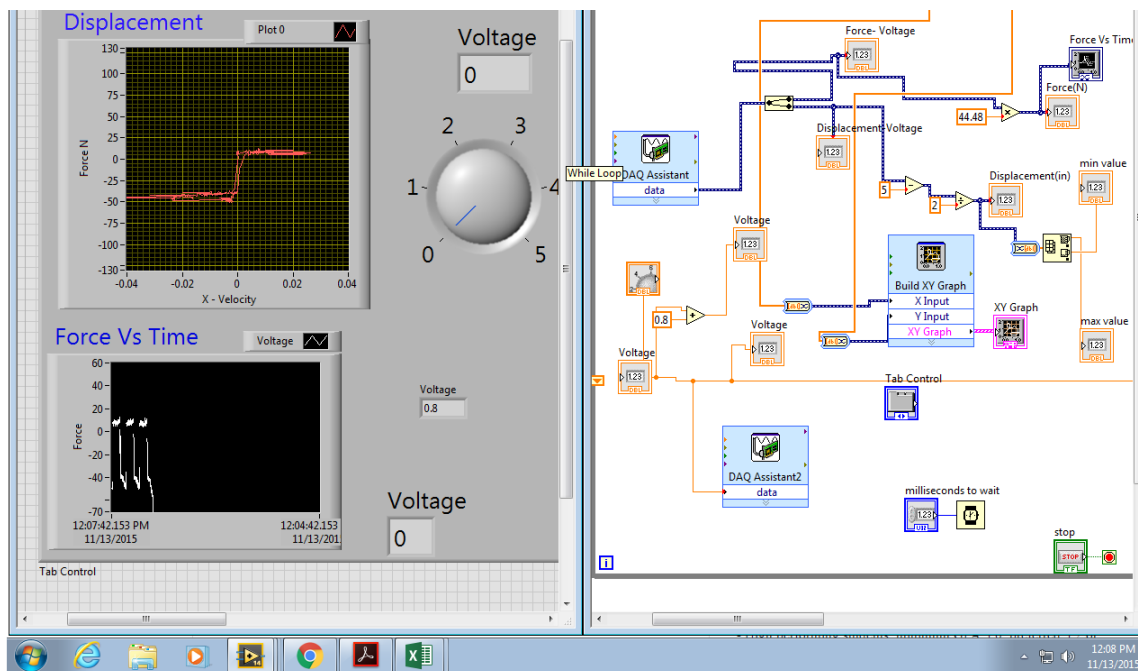
Figure 10.3 Force vs velocity plot for 1V
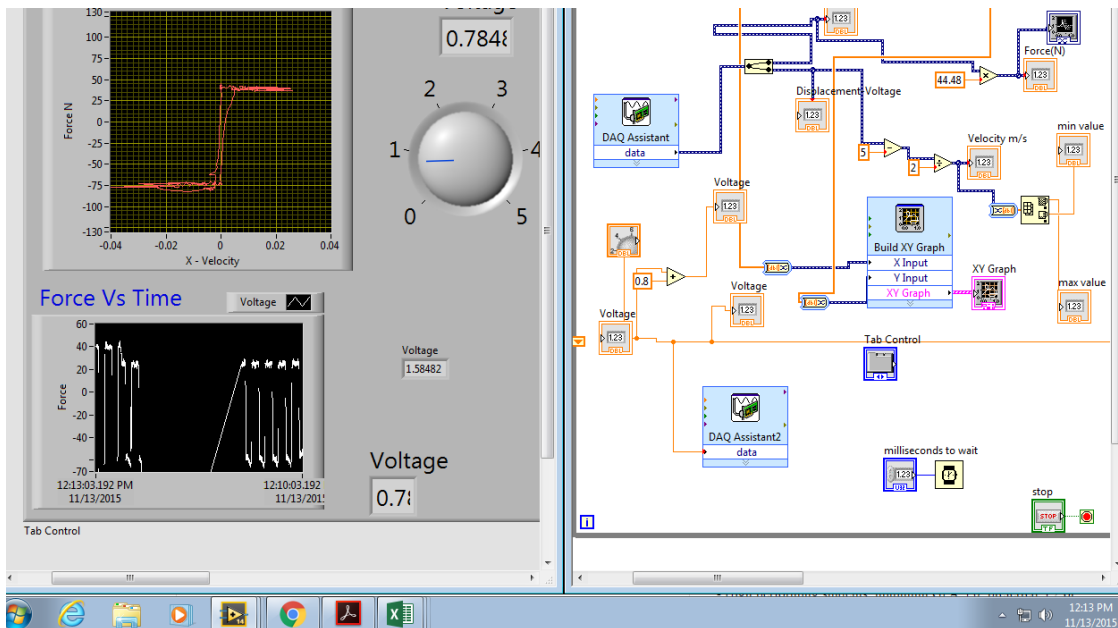
Figure 10.4 Force vs velocity plot for 0.7V
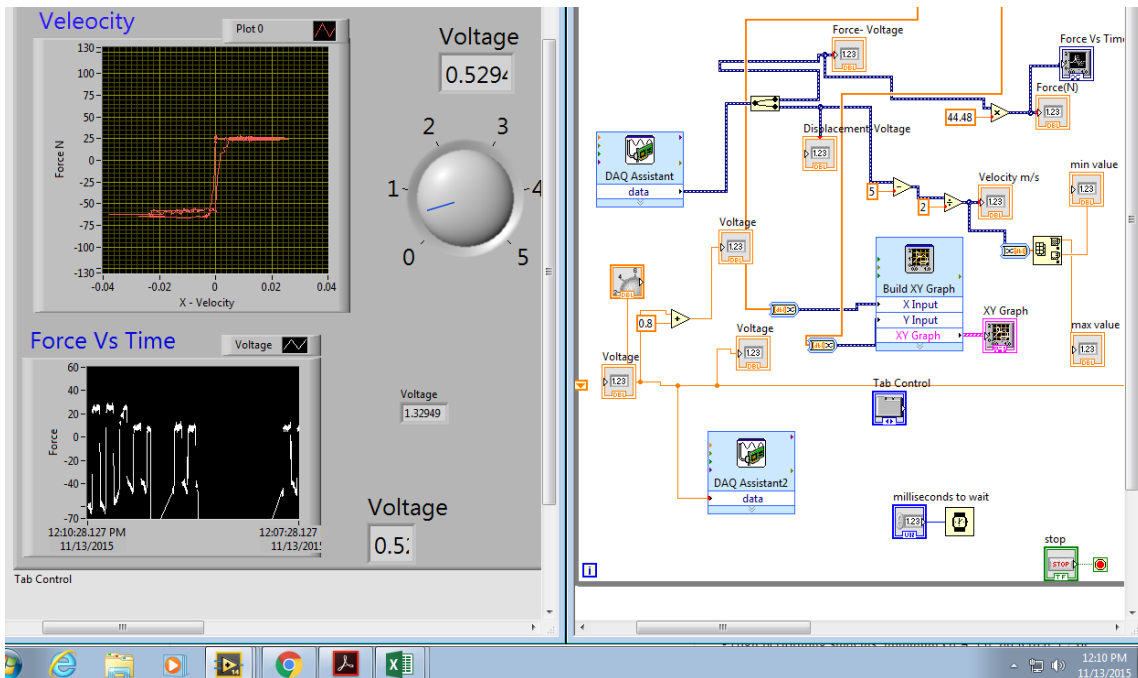
Figure 10.5 Force vs velocity plot for 0.5V

Figure 10.6 Force vs velocity plot for 0V

B. Appendix- Experimental force vs displacement plot

The force vs displacement plots for different voltage values are shown in the below Figure 10.7, 10.8, 10.9, 10.10, 10.11, 10.12.
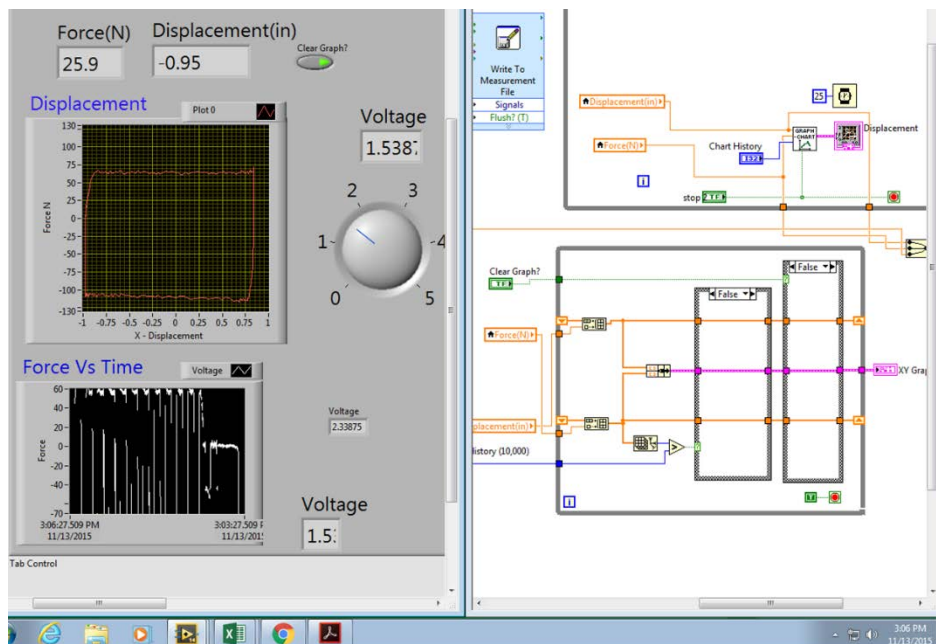

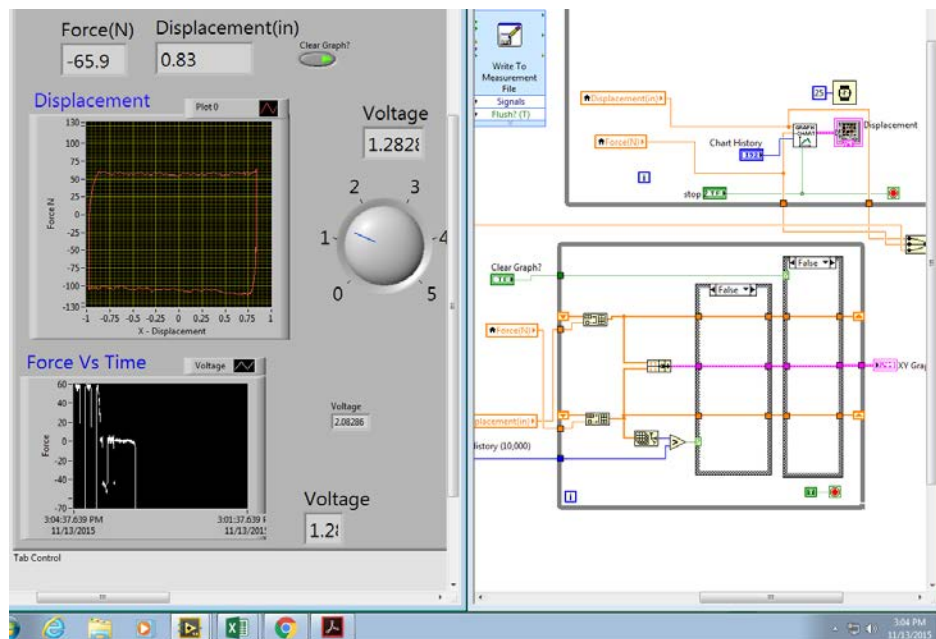Figure 10.7 Force vs displacement plot for 1.5V
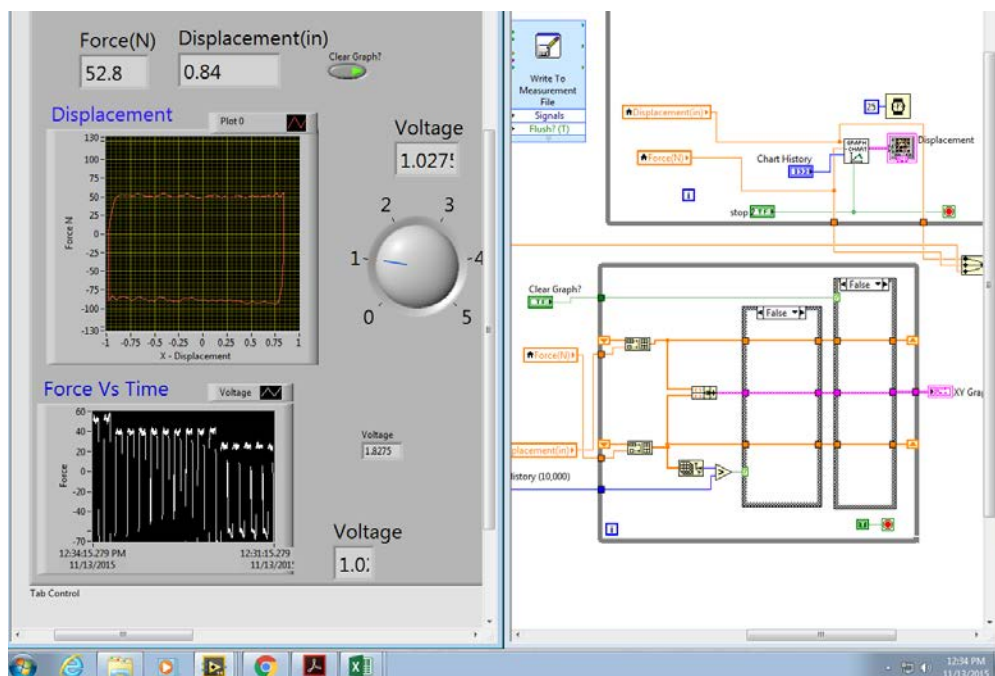

Figure 10.8 Force vs displacement plot for 1.2V

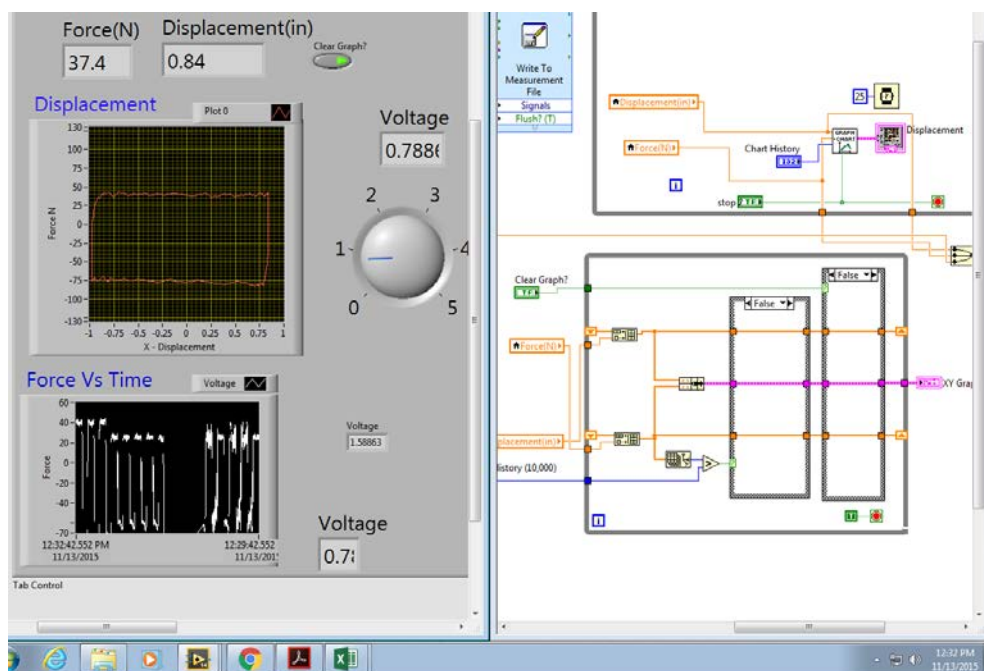Figure 10.9 Force vs displacement plot for 1V
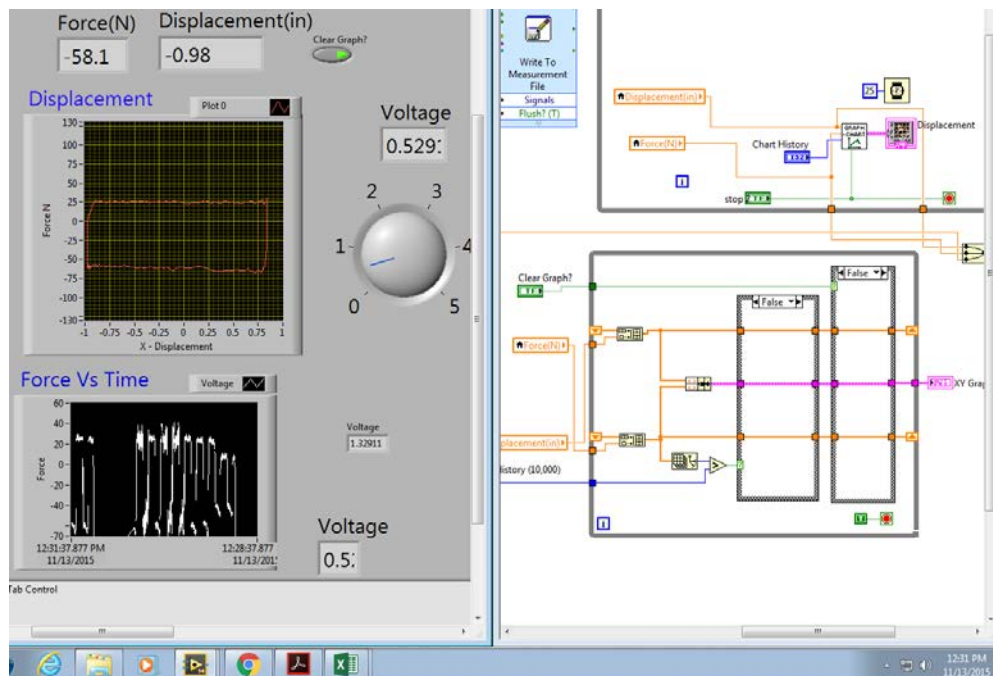

Figure 10.10 Force vs displacement plot for 0.7V

Figure 10.11 Force vs displacement plot for 0.5V